Marine Environmental Research 192 (2023) 106241

Contents lists available at ScienceDirect

Marine Environmental Research

journal homepage: www.elsevier.com/locate/marenvrev

Impact of hydrodynamics on community structure and metabolic production of marine biofouling formed in a highly energetic estuary

Aurélie Portas [a,b], Nathan Carriot [b], Annick Ortalo-Magné [b], Guillaume Damblans [a], Maxime Thiébaut [a], Gérald Culioli [b,c], Nolwenn Quillien [a], Jean-François Briand [b,*]

[a] France Energies Marines, Plouzané, France
[b] MAPIEM, EA 4323, Université de Toulon, France
[c] IMBE, Aix-Marseille Université, Avignon Université, CNRS, IRD, Avignon, France

ARTICLE INFO

Keywords:
Shear stress
Biofouling
Microbial community
Metabolomics
Extracellular polymeric substances (EPS)

ABSTRACT

Biofouling is a specific lifestyle including both marine prokaryotic and eukaryotic communities. Hydrodynamics are poorly studied parameters affecting biofouling formation. This study aimed to investigate how water dynamics in the Etel Estuary (Northwest Atlantic coasts of France) influences the colonization of artificial substrates. Hydrodynamic conditions, mainly identified as shear stress, were characterized by measuring current velocity, turbulence intensity and energy using Acoustic Doppler Current Profiler (ADCP). One-month biofouling was analyzed by coupling metabarcoding (16S rRNA, 18S rRNA and COI genes), untargeted metabolomics (liquid chromatography coupled with high-resolution mass spectrometry, LC-HRMS) and characterization of the main biochemical components of the microbial exopolymeric matrix. A higher richness was observed for biofouling communities (prokaryotes and eukaryotes) exposed to the strongest currents. *Ectopleura* (Cnidaria) and its putative symbionts *Endozoicomonas* (*Gammaproteobacteria*) were dominant in the less dynamic conditions. Eukaryotes assemblages were specifically shaped by shear stress, leading to drastic changes in metabolite profiles. Under high hydrodynamic conditions, the exopolymeric matrix increased and was composed of 6 times more polysaccharides than proteins, these latter playing a crucial role in the adhesion and cohesion properties of biofilms. This original multidisciplinary approach demonstrated the importance of shear stress on both the structure of marine biofouling and the metabolic response of these complex communities.

1. Introduction

In marine environments, biofouling refers to the complex colonization of submerged substrates by micro- and macro-organisms (Railkin, 2003). This biological process consists on adhesion and diversification of microbial communities, dominated by bacteria, diatoms, and other unicellular eukaryotes, embedded in a self-produced matrix of extracellular polymeric substances (EPS), followed by the settlement of larger multicellular organisms (Dobretsov and Rittschof, 2020; Flemming and Wingender, 2010). The unwanted development of biofouling is an issue for marine industry, as it leads to increased costs and more regular maintenance operations (Davidson et al., 2023; Schultz et al., 2011). In the offshore renewable energy sector, biofouling affects different components (e.g., dynamic cables, mooring lines, floats) by influencing hydrodynamic behavior or increasing structural loads, which finally can negatively affect structural resistance and energy production (Want et al., 2021). However, research in this domain is scarce due to limited access to structures deployed in highly dynamic offshore environments.

Regardless of their sessile way of life, the composition of biofouling communities is controlled by a wide range of environmental parameters, physicochemical properties of substrates and biological interactions (Antunes et al., 2019; Briand et al., 2017; Dang and Lovell, 2016). In recent decades, most of the studies in this research field have investigated the relationships between marine biofouling communities and environmental variables, such as salinity (Song et al., 2022), nutrients (Lawes et al., 2016), temperature (Briand et al., 2017), and trace metal elements concentrations (Djaoudi et al., 2022). Conversely, knowledge of how hydrodynamics mediate biofouling formation in the field is limited. Hydrodynamics is induced by the flow surrounding the substrate and it is the sum of the incoming flow and the local wake, i.e., the flow modification due to the presence of the substrate and the biofouling itself. Biofouling is therefore sensitive to flow dynamics but it also modifies the surrounding flow (Marty et al., 2022). Hydrodynamic loading is of three-dimensional nature in the turbulent regime and

* Corresponding author.

https://doi.org/10.1016/j.marenvres.2023.106241
Received 19 June 2023; Received in revised form 2 October 2023; Accepted 23 October 2023
Available online 27 October 2023

therefore presents two categories of loadings: normal and tangential forces. Normal forces are expressed as pressure fields, and they are typical of oscillating flows, such as waves acting on offshore systems. Tangential forces represent shear stress; these forces are typical of tidal hydrodynamics or ships in transit. In this study, we focused on the impact of shear stress on biofouling communities.

Previous studies have mainly focused on the effects of shear stress on bacterial biofilms formed with cultures of pathogenic strains or in freshwater ecosystems in controlled conditions and using cultures of isolated strains (Chun et al., 2022; Simões et al., 2022; Tsagkari et al., 2022). All these studies show that flow forces can have a very strong influence on biofilms. For example, shear stress influences the attachment of organisms (Kastl et al., 2020), the oxygen supply (Thames et al., 2023), the composition of communities (Catão et al., 2019; Schmidt et al., 2018), the structure (Battin et al., 2003) and the metabolism of biofilms (Jones and Buie, 2019). Moreover, local hydrodynamics associated with the specific properties of the natural environment can also influence the organization of the biofilm matrix. These observations have been particularly well demonstrated for *Pseudomonas aeruginosa* biofilms which form large and stiff 3D structures when subjected to high hydrodynamic forces (Nadell et al., 2017). In general, biofilms grown under high shear conditions have a flat and dense monolayer structure, which is able to withstand mechanical stress due to its compactness. Conversely, under low shear conditions, biofilms have a multilayer structure which improves nutrient exchange compared to the flat structure, but they cannot resist the same mechanical stimuli (Araújo et al., 2016; Liu and Tay, 2002; Paul et al., 2012). Furthermore, in natural aquatic ecosystems, it has been reported that the flow force exerted on stream biofilms alters biofilm community assembly, with flow-induced changes affecting community richness (Besemer et al.,

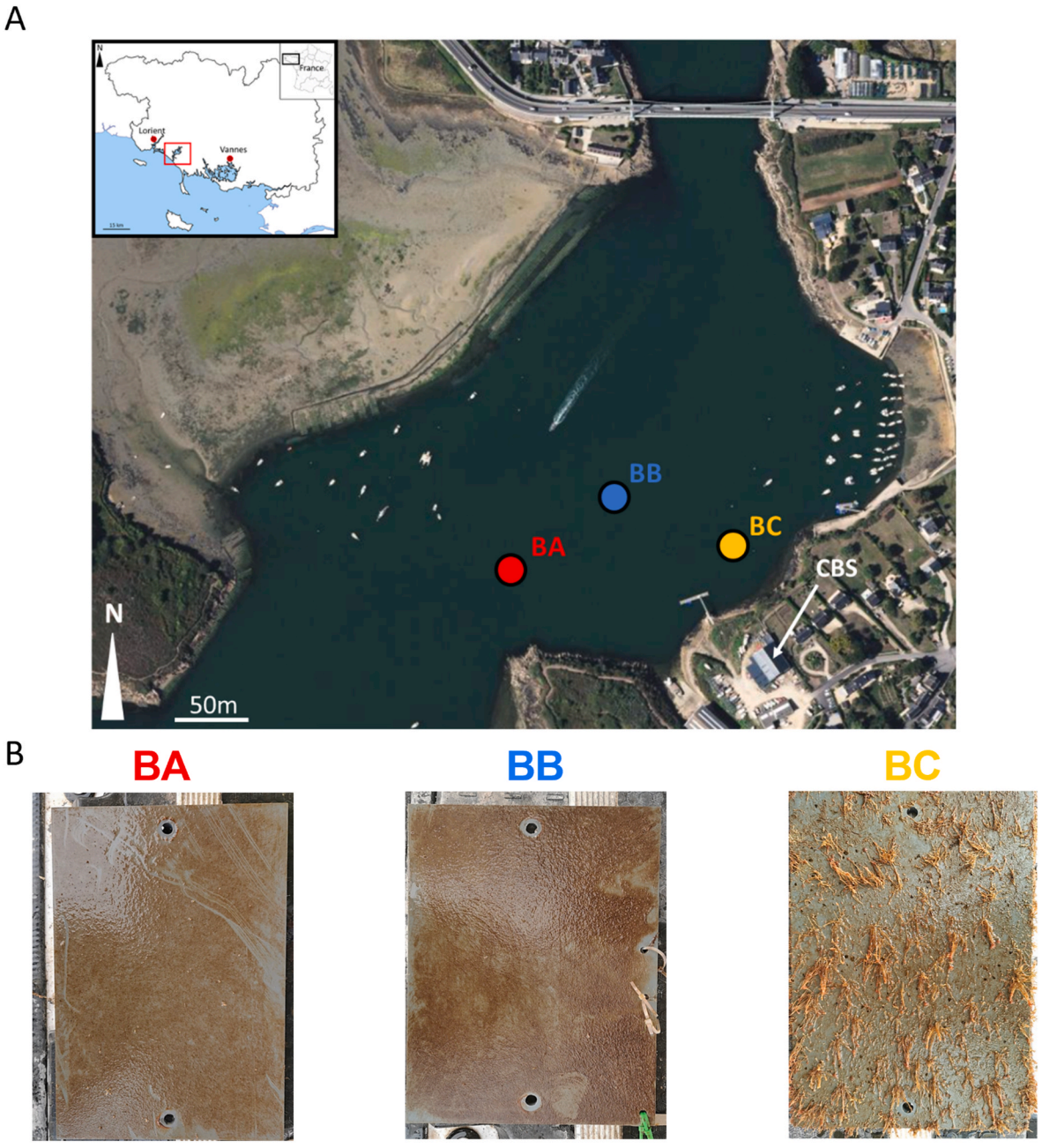

Fig. 1. Map of the sampled sites and photographs of panels (A). Map of the sampling area in the Etel estuary. Colors show sampled sites [red: buoy A (BA), blue: buoy B (BB), and orange/yellow buoy C (BC)]. **(B)** Photographs of the panels sampled at each site after 27 days of immersion.

2007). Therefore, to date, the knowledge on the relationships between shear stress and marine biofouling communities is very sparse and, moreover, limited to prokaryotes or diatom communities (Catão et al., 2019; Zargiel et al., 2011). Especially, few studies have described the whole biofouling assemblages, including microbes and multicellular eukaryotes, formed *in-situ* under hydrodynamic stress.

Thus, the aim of this study was to understand the effects of a complex estuarine hydrodynamic regime characterized by strong marine currents on biofouling prokaryotic and eukaryotic assemblages. This *in-situ* experiment was conducted at the estuary of the Etel River (French Atlantic coast, Brittany) as this site is characterized for strong tidally driven currents (up to 2.5 m/s) (Thiébaut et al., 2022). The mean discharge of the Etel river is 4.5 m^3/s, which is in the same order of magnitude as more than 30 other French estuaries, representing nearly 60% of all French estuaries. A combined multidisciplinary approach including metabarcoding, biochemical composition of the matrix and metabolomics, aimed to provide complementary information on the effect of shear stress on the biofouling process in a natural environment.

2. Materials and methods

2.1. Study site and experimental design

The Etel estuary is located on the Northwest Atlantic coasts of France (Brittany; 47°67′N; 3°20′W). The hydrodynamic regime of the river is mainly controlled by tides. Three sampling sites were selected to study different hydrodynamic conditions in the Etel estuary. Two of them (buoys BA and BB) are high-energy sites located in the center of the river (buoys BA and BB) while the third site (buoy BC) is located close to the shoreline (Fig. 1A). Buoys BA, BB and BC were immersed at 11.8, 10.2 and 8.7 m depth. BA was the westernmost buoy (78 m from shore), BB was the northernmost buoy (137 m from shore), and BC was in the east, (47 m from shore). There is 30 m between two adjacent buoys.

The experiment was conducted in 2020 for one month (from 13 October to 10 November). Each buoy had a vertical metal frame supporting 6 polyvinylchloride (PVC) panels (20 cm × 27 cm) at 1.5m depth (Fig. S1). All the panels were sandblasted to increase roughness and promote adhesion. The PVC plates were used as biocolonisation supports. After 27 days of immersion, biofouling material was collected from the panels using sterile stainless-steel blades. Three replicates were scrapped for each analysis (Fig. S2).

2.2. Environmental data collection

Water temperature, turbidity, salinity, and dissolved oxygen (DO) concentration measured *in-situ* were provided by the REPHY program (REPHY – French observation and monitoring program for phytoplankton and hydrology in coastal waters, 2021). The measurements were carried out 3 times during the immersion period upstream of the Lorois bridge (300 m from the studied sites). Seawater was also collected and transported to the laboratory. Nutrients (NO_2^-, NO_3^-, PO_4^{3-}, $Si(OH)_4$) were measured using standard colorimetric methods for seawater while dissolved organic carbon (DOC) and total nitrogen (TN) were analyzed on a TOC-V_{CSH} analyzer (Shimadzu) (Oursel et al., 2013).

2.3. Hydrodynamic conditions

Velocity measurements from three 5-beam ADCP (Nortek Signature 1000 kHz) were used to assess the flow dynamics and turbulence within the Etel estuary. Further details of the ADCP configuration deployments and the assessment of flow dynamics and turbulence at the Etel estuary sites have been previsouly described in Thiébaut et al. (2022).

In this paper, the metrics of interest for the flow characterization were: flow (streamwise) velocity, turbulence intensity (TI) and turbulence kinetic energy (TKE) throughout the water column. TI is referred to as the turbulence level and represents the intensity of velocity fluctuations. It is expressed as the ratio of the standard deviation of the streamwise velocity within a 10 min flow velocity subset to the mean flow velocity of the same subset (e.g., Sentchev et al., 2020). It is represented as a percentage. TKE is the average kinetic energy associated with eddies in turbulent flow. TKE is determined as half of the variance in flow velocity calculated over 10 min subsets.

The ADCPs were deployed for two different periods to cover the three sites. Firstly, for 24 days, from 12 September to 6 October 2020, where the ADCPs were deployed on the seafloor, below the BA and BC buoys. Second, for 27 days, from 13 October to 10 November 2020, a single ADCP was deployed on the seafloor below buoy BB (corresponding to the immersion panel period).

2.4. DNA metabarcoding, bioinformatics and statistical analysis

DNA was extracted using the DNeasy PowerBiofilm Kit (Qiagen) according to the manufacturer's instructions. A negative control was included in the extraction protocol. DNA quantity and quality were measured using NanoDrop 1000 spectrophotometer (ThermoScientific).

Three sets of primers were selected for metabarcoding: the V4-V5 region of the 16S rRNA gene for prokaryotes (Parada et al., 2016), while eukaryotic diversity was analyzed using two genetic markers best adapted to marine biofouling communities (Portas et al., 2022): the mitochondrial cytochrome *c* oxidase I (COI) (Leray et al., 2013) and the V7 region of the 18S rRNA gene (Gast et al., 2004; Van de Peer et al., 2000). Primers were modified to include Illumina™ overhang adaptors. Primer sequences and PCR programs are detailed in the Supporting Information (DNA metabarcoding and sequencing section). Negative controls were performed for the three markers. Samples (n = 27, 9 per each primer pair) were sequenced on the Illumina MiSeq platform with the 2 × 300 bp chemistry (Eurofins Genomics, Ebersberg, Germany). All data are available from the NCBI BioProject database (accession number PRJNA883975).

Adapters were first removed using Cutadapt v.3.1 (Martin, 2011). Reads were filtered, dereplicated, merged and chimera were removed using DADA2 v.1.20.0 (Callahan et al., 2016) in R software and ASVs (Amplicon Sequence Variant) were assigned using the FROGS v.4.0.1 (Escudié et al., 2018). For bacteria, ASVs were assigned using the SILVA 138 database. The Protist Ribosomal Reference (PR2, v.4.14.0) was used for 18S rRNA sequence assignment and BOLD (v.2022) for the COI sequences, the latter containing only marine sequences. ASV sequences were assigned using blast+ (v.2.10), retaining ASVs with ≥75% sequence coverage and ≥95% identification for both 16S rRNA and 18S rRNA data, and ≥80% for COI. Below these thresholds, an ASV was classified as unknown if it had a bootstrap confidence score below 65% at any level using the naive Bayesian classifier method (Wang et al., 2007). Subsequently, ASVs with an abundance lower than 0.005% (Bokulich et al., 2013) and sequences not assigned to marine species (i.e., contamination by human DNA and terrestrial species) were removed from the dataset. ASVs classified as chloroplast or mitochondrial were removed from the 16S rRNA gene dataset.

Statistical analyses were performed in R implementing the *phyloseq* (McMurdie and Holmes, 2013) and *vegan* (Oksanen et al., 2009) packages. Samples were rarified to the minimum sample read depth for each primer (16S rRNA gene: 27,631; 18S rRNA gene: 141,902; COI: 70,205). As estimates of relative eukaryotic abundance could be biased by variation in the length and number of copies of this gene between eukaryotic taxa, the analyses were based on presence/absence indices. For this reason, alpha diversity was calculated from Chao1 richness and the number of ASV observed. The effects of tidal flow on biofouling species richness were tested using an analysis of variance (ANOVA) followed by Tukey's honestly significant difference test. Beta diversity was examined using a Principal Coordinate Analysis (PCoA) ordinations based on the weighted UniFrac dissimilarity matrix for prokaryotic data and on the unweighted UniFrac distance matrix for eukaryotic data. Permutational analyses of variance (PERMANOVA) with "sampling site" as a factor and

pairwise comparisons were performed. Additionally, to identify the taxa associated with hydrodynamic conditions, differential abundance (log fold changes; LFC) of genera between high (BA and BB) and low (BC) hydrodynamic conditions was performed using DESeq2 (Love et al., 2014). Count data were normalized by a regularised logarithmic transformation, which accounts for lower counts.

To investigate potential interactions between bacterial communities and eukaryotes from biofouling, a cooccurrence network was created with CoNet (Faust and Raes, 2016). For this analysis, samples belonging to the 18S rRNA gene and 16S rRNA sequences were included. Pearson and Spearman correlations, mutual information and Bray-Curtis dissimilarities were calculated. P values were further computed from method- and edge-specific permutations and bootstrap score distributions with 1000 iterations each. The initial top and bottom edge numbers were set at 150. Correction for multiple-testing of the *p*-values was performed according to Brown's method followed by Benjamini-Hochberg correction. Networks were analyzed using Cytoscape, v 3.9.1.

2.5. Metabolomics analysis

The biological material was transferred to a glass tube containing 25 mL of pure ethyl acetate (analytical grade; Carlo Erba; Val-de-Reuil, France) and stored at 4 °C until further laboratory analysis. For medium blanks (in triplicate), a PVC panel without colonization was treated according to the same protocol. The 12 samples were then sonicated in an ultrasonic bath (Bransonic 2150E-DTH; Danbury, CT, USA) for 30 min at room temperature. The upper organic phases were collected in separate glass tubes and dried under N_2. The tubes were then filled with argon and stored at −20 °C. All dried extracts were weighed, dissolved in LC-MS grade methanol (Fisher; Loughborough, UK) to a final concentration of 10 mg/mL for each sample, and then transferred in 2 mL-HPLC vials.

A pool sample solution was prepared by taking an aliquot of each sample (biofouling extracts and medium blanks). The resulting solution was divided into several HPLC vials, which were used as quality control (QC) samples to ensure reproducibility. Prior to injection, all samples, blanks, and QCs were filtered (0.22 μm). At the beginning of the injection sequence, two analytical blanks (methanol only) and a QC sample (× 10) were injected before the samples. Biofouling extracts and media blanks were then injected randomly to avoid possible time-dependent changes in LC-MS chromatographic fingerprints, while a QC sample was injected every three samples.

Biofouling metabolome analyses were performed on an ultra-performance liquid chromatography system coupled to an electrospray ionization quadrupole time-of-flight mass spectrometer (UHPLC-ESI-QTOF-MS) in positive mode. All characteristics are detailed in the Supporting Information (Metabolomics section).

LC-MS raw data were converted into ".netCDF" files using DataAnalysis (version 4.3; Bruker Daltonics) and processed using MZmine-2.58 (Pluskal et al., 2010). The first step corresponded to the final data matrix construction, with parameters listed in Table S1. In a second step, two successive filtering steps were applied to remove experimental and analytical biases based on signal-to-noise ratio (using blanks; minimal S/N ratio: 6) and coefficient of variation (using QCs; minimal CV: 20%) with an in-house script on R and final manual filtering. The resulting data matrix was analyzed using the MetaboAnalyst 5.0 online webtool (Chong et al., 2018). Data were normalized using log10 transformation and mean-centered for better comparability. Principal component analysis (PCA) was performed to visualize the inherent clusters between conditions, and partial least squares discriminant analysis (PLS-DA) to assess the discrimination between groups and to characterize chemomarkers of each group. From the PLS-DA, variable importance in projection (VIP) values were selected to assess the importance of each metabolite in driving the separation between groups.

2.6. Metabolites annotation using molecular networking

Data analysis software was used to convert raw UPLC-MS/MS files into ".mzXML" files. These MS/MS data were used to build a molecular network (MN) using the Global Natural Products Social Molecular Networking online workflow (GNPS web platform; http://gnps.ucsd.edu). This platform allows creating a network to visualize compounds with similar chemical structure based on the similarity of their tandem MS/MS fragmentation patterns (Wang et al., 2016). The creation of a restricted MN was conducted to annotate the largest number of metabolites (see Carriot et al. (2021) and Table S2). For this purpose, the parameters used were precursor ion mass tolerance (Da): 0.02; fragment ion mass tolerance (Da): 0.02; minimum cosine score: 0.70; minimum matched fragment ions: 4; network TopK: 10. Data from GNPS platform were imported into Cytoscape (v.3.8.0) for MN visualization. Metabolites present in blank samples were manually eliminated from the MN. Metabolites annotation was done according to Carriot et al. (2022).

2.7. Extraction and characterization of EPS

To analyze the EPS matrix, the biofouling material was scrapped using sterile stainless-steel blades and transferred to a sterile 50 mL Falcon tube containing 10 mL of Artificial Sea Water (36 g/L of sea salts, Sigma Aldrich). A series of centrifugations and precipitations were carried out to extract the different fractions of EPS (D'Abzac et al., 2010; More et al., 2014). First, sample tubes were briefly vortexed and then centrifuged at high speed (30 min; 4 °C; 20,000 *g*). The resulting supernatants containing extracted EPS were transferred into sterile 50 mL Falcon tubes with 3 vol of ice-cold ethanol at 95 % and incubated overnight at −20 °C. After incubation, the tubes were centrifuged at 20, 000 *g* for 30 min at 4 °C. The supernatants were removed, and the precipitated EPS pellets were freeze-dried before being weighed. They represented the colloidal fraction of EPS (CF). In a second time, the pellets from the first centrifugation of sample tubes were resuspended in 5 mL ASW, briefly vortexed and sonicated for 3 min at 100 W. The samples were then centrifuged at 20,000 *g* for 30 min at 4 °C. The pellets corresponded to the residual fraction (RF, consisting of intact cells and other residues). The supernatants were treated using the same protocol as before to obtain, as precipitated compounds, the bound fraction of EPS (BF, potentially including some intracellular polymers). Finally, BF and RF fractions were freeze-dried before being weighed. For each immersed panel, the biofilm biomass was correlated to the sum of fraction weights (CF, BF and RF).

To determine the total chemical composition of the different fractions, they were dissolved in water at a concentration of 2 mg/mL. The protein content was determined by the Bradford method (Bradford, 1976) using BSA as standard. The carbohydrate content was determined by the phenolsulphuric acid method (Dubois et al., 1956) and the uronic acid content by the metahydroxyphenyl method (Blumenkrantz and Asboe-Hansen, 1973) using glucose and glucuronic acid as standards, respectively. For all these tests, EPS solutions were transferred in triplicate to a transparent 96-well microplate. Optical densities were measured using a plate reader (TECAN, Infinit 200 Pro).

3. Results

3.1. Physico-chemical and hydrodynamic characteristics of Etel estuary

Temperatures and dissolved oxygen ranged from 15.2 ± 2.9 °C and from 7.9 ± 0.9 °C, respectively (Table S3). Salinity and TN were stable (mean 34.8 and 0.3 mgN/L, respectively). In contrast, the Etel site showed high variations in nutrient measurements, especially for DOC (2.2 ± 2.6 mgC/L), SiO_2 (8.6 ± 5.1 μM), and NO_3^- (5.2 ± 3.3 μM).

The three sites differed in levels of hydrodynamic disturbance as indicated by velocity and turbulence measurements (Table 1). BA and BB were exposed to strong currents (up to 2.43 and 2.47 m/s,

Table 1
Hydrodynamic parameters (i.e., flow velocity, turbulent intensity, and turbulent kinetic energy) at 3 Etel sites (BA, BB et BC) measured monthly from September 2020 to October 2020 for BA and BC and from October 2020 to November 2020 for BB. The table shows the maximum, minimum, mean, and standard deviation values of each hydrodynamic variable.

Variable	B_A				B_B				B_C			
	Max	Min	Mean	SD	Max	Min	Mean	SD	Max	Min	Mean	SD
Flow velocity (m/s)	2.43	0	0.74	0.65	2.47	0.01	0.83	0.56	0.93	0.01	0.25	0.15
Turbulence intensity (%) - TI	33.35	0.17	3.2	2	29.99	0.22	2.89	1.38	27.8	0.16	3.62	3.17
Turbulent Kinetic Energy (m^2/s^2) - TKE	0.45	0	0.04	0.04	0.23	0	0.03	0.03	0.2	0	0.02	0.02

respectively) whereas those recorded near BC reached only 0.93 m/s. Furthermore, turbulent kinetic energy (TKE) values were higher at BA than at the other sites. Turbulence intensity (TI) was similar between the 3 sites with large variations.

3.2. Biofouling community structures

The raw sequence data from 18 samples resulted in 1,342,341 16S rRNA sequences, 2,688,794 18S rRNA gene reads and 1,232,952 COI reads. In the final rarified dataset, the number of assigned ASVs was also uneven: 1378 ASVs for the 16S rRNA gene, 459 ASVs for the 18S rRNA gene and 784 ASVs for the COI gene. The rarefaction curves reached saturation for the detected ASVs, indicating that the coverage was sufficient (Fig. S3).

The richness measured by Chao1 for prokaryotic communities was significantly different between the three sites (ANOVA, $p < 0.05$) (Fig. 2A). In contrast, alpha diversity indices for eukaryotic communities varied similarly regardless of the gene (18S rRNA gene and COI), with the lowest richness at BC but no significant differences between BA and BB. The same result was observed for the number of ASVs detected (Fig. S4).

Overall, beta diversity showed a similar pattern for bacterial and eukaryotic communities (Fig. 2B). Community composition was similar in BA and BB, but significantly different in BC, regardless of the gene sequenced (PERMANOVA, $p < 0.05$). Axis 1 represented between 53 and 76% of the variability, regardless of the gene used.

Across all sites, a wide diversity of foulers was identified (Figs. 1B and 3). For bacteria, *Alphaproteobacteria*, *Bacteroidia*, *Gammaproteobacteria* and *Verrucomicrobiaea* were the most abundant genera in BA and BB samples. The most abundant group in BC samples was an unknown genus (*Gammaproteobacteria*, order *Pseudomonadales*). Moreover, only one ASV of *Candidatus Nitrosopumilus* archaea was represented in the dataset, with only 0.04% sequence reads. Despite these differences, 75% of the genera were shared between the three sites, accounting for over 98% of the total number of reads (Fig. S5A). Conversely, approximately 44% of eukaryotic genera were shared between the three sites, and this proportion represented an average of 88% and 87% of the total number of reads for 18S rRNA and COI, respectively (Figs. S5B and S5C). Among 18S rRNA gene and COI datasets, arthropods belonging to the genera *Harpaticus* and *Jassa*, as also *Ectocarpus* (Phaeophyceae) were more abundant at the BA site, while Bacillariophyta, especially *Navicula* and *Shionodiscus*, were abundant at the BB site. *Rhabditophanes* (Nematoda), identified using COI data, were particularly abundant in BA and BB samples. The BC samples were composed of Arthropoda and Cnidaria,

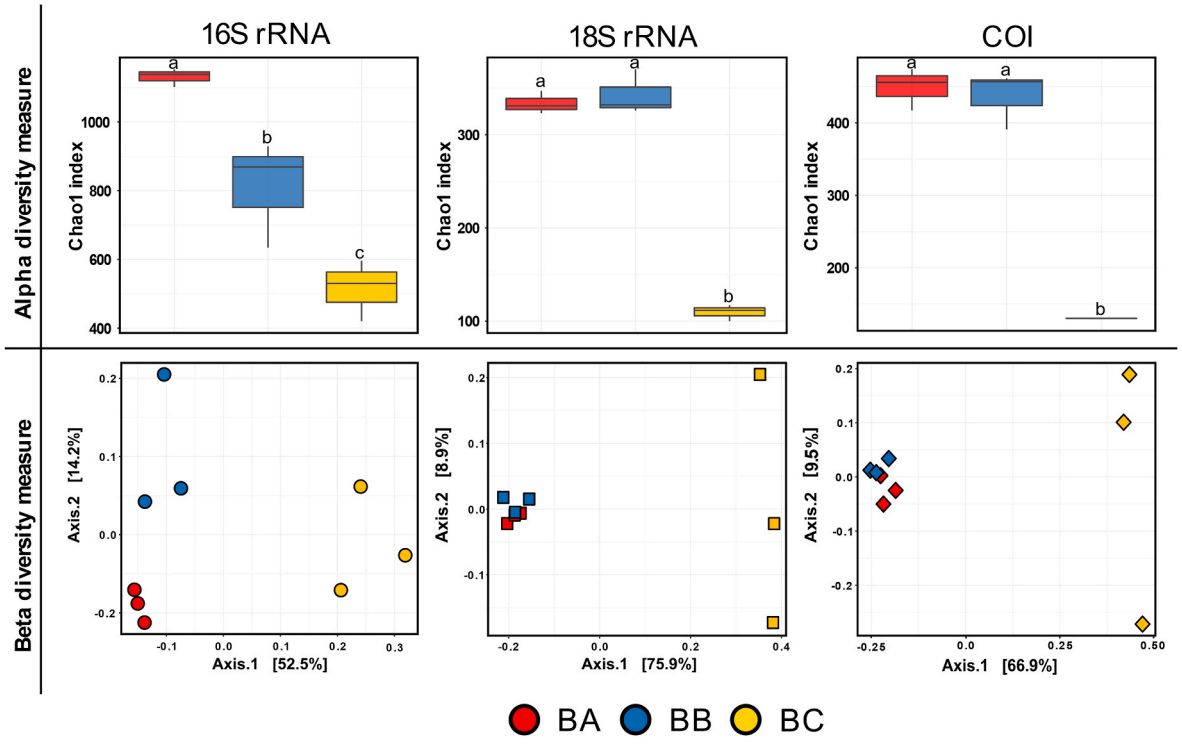

Fig. 2. Distribution of alpha- and beta-diversity of the biofouling communities according to the 3 Etel sites (BA, BB and BC). (A) Boxplots of the Chao1 index at the ASV level at each site obtained from 16S rRNA gene, 18S rRNA gene and COI. The line in each box plot indicates the median, the box delimits the 25th and 75th percentiles, and the whisker corresponds to the full range. Letters above boxplots represent pairwise comparisons between each site. **(B)** PCoA of biofouling composition across different primers (shapes) and at different sites (colors). Weighted Unifrac distances were used for 16S rRNA gene while unweighted Unifrac distances were used for both 18S rRNA and COI gene. Each point represents one sample.

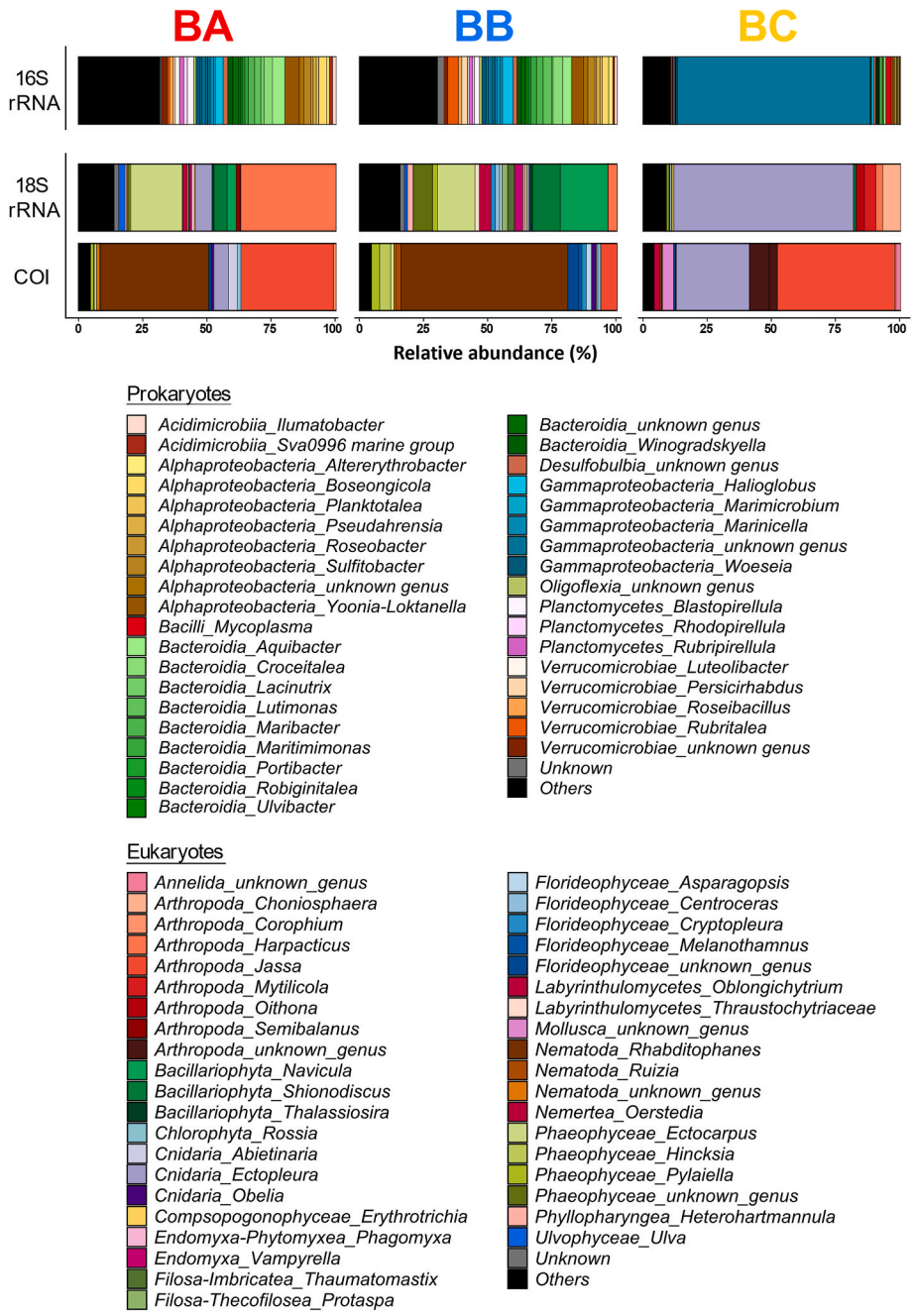

Fig. 3. Composition of the marine fouling communities at the 3 Etel sites (BA, BB and BC). Taxonomic composition obtained from 16S rRNA, 18S rRNA and COI genes analyses at the genus level (relative abundance >0.05%).

mainly represented by the genera *Ectopleura* and *Jassa*.

3.3. Differential community analysis depending on hydrodynamics

Due to taxonomic and hydrodynamic similarities, samples BA and BB were considered to be exposed to high and BC to low hydrodynamic conditions. Accordingly, a differential analysis was performed to identify genera specifically associated with low and high hydrodynamic regimes. The DESeq2 results showed that some members of the *Alphaproteobacteria*, such as *Neorickettsia* or *Albimonas*, were more abundant in the low current samples. *Gammaproteobacteria* were also abundant with 5 genera identified in the BC samples, including *Marinomonas*, *Francisella* and some genera of the *Pseudomonadales* which includes *Endozoicomonas* genus (Fig. 4A). Conversely, a significant increase in relative abundance was observed for *Aureispira*, OM27 clade, *Propionigenium* or *Roseobacter* in samples exposed to high flows.

Among the eukaryotic communities, genera discriminating under low current conditions were identified as members of *Kallimenia* (Florideophyceae), *Ectopleura* (Cnidaria), and *Bastodinium* (Dinophyceae), but also several arthropod genera such as *Phtisica* and *Caprella* which showed a high LFC values (Fig. 4B). Conversely, taxa which were differentially abundant under strong current conditions belong to the class Bacillariophyta, including the genera *Navicula* and *Nitzschia*. Other genera of the classes Discosea-Flabellinia, Endomyxa, Filosa-Thecofiliseo, Labyrinthulomycetes, Phyllopharyngea and Phaeophyceae, including the genus *Pylaiella*, were also abundant under high current conditions.

To explore the relationship between the eukaryotic and bacterial

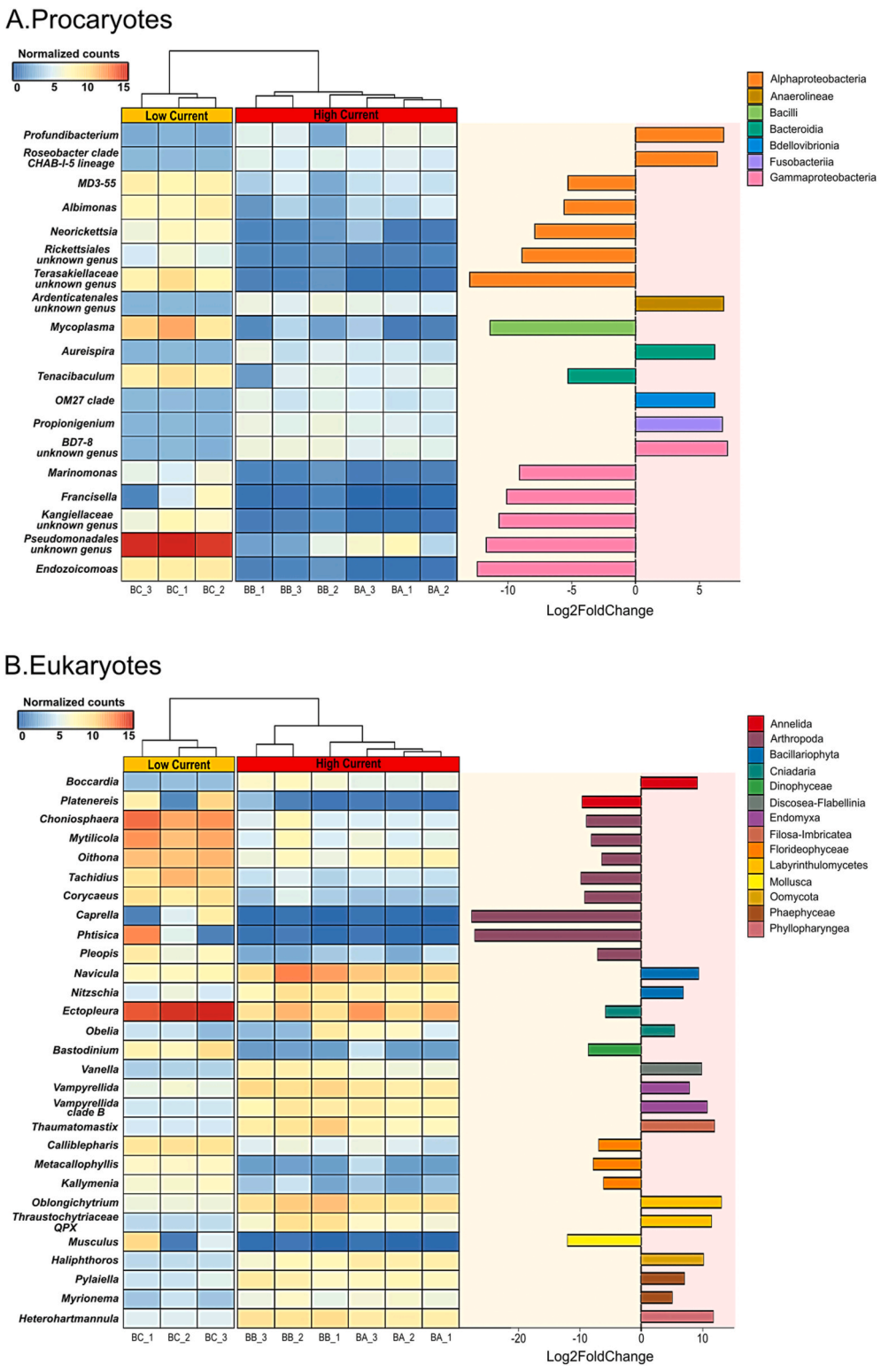

Fig. 4. Differential analysis of genera obtained using DeSeq2 between the most abundant and discriminant taxa in low and high flow regimes. Heatmap of differential abundance of genera (given as log2 normalized counts) and barplots of Log2 fold changed values obtained for **(A)** prokaryotes and **(B)** eukaryotes. Eukaryote communities include COI and 18S rRNA gene taxa. A gradient from blue to red indicated genus abundance across sites. Barplots show Log2 fold changed values, positive values indicate an increased presence in low current and negative values indicate presence in high current. Only genera with a significance level lower than 0.001 (FDR-adjusted DESeq2 *p*-values), and Log2 fold change values higher than 5 are shown. Genera are grouped according to the class level.

communities, a co-occurrence network analysis was performed and revealed three distinct clusters (Fig. S6). A high number of ASV occurrences were found in samples BA and BB, representing 85 nodes associated with 112 edges. In cluster A, ASVs associated with *Ulva* had the highest number of positive links and were correlated with bacteria such as *Roseovarius*, *Aquibacter*, *Luteolibacter* and *Yoonia-Loktanella*. For cluster B, the highest number of edges corresponded to 4 eukaryotes belonging to the Bacillariophyta, including two raphid pennate

(*Nitzschia* and *Cocconeis*) and two polar centric diatoms (*Shionodiscus* and *Minidiscus*). These ASVs were positively correlated with bacterial genera including several members of the *Verrucomicrobiales*, such as *Persicirhabdus* and *Rubritalea*. Cluster C consisted of ASV mainly found in BC samples with the presence of two bacteria (*Pseudomonales* and *Fokiniaceae*) and three eukaryotes (*Oithona*, *Calliblepharis* and *Ectopleura*).

3.4. Variations of metabolites in biofouling samples

A UHPLC-(+)-ESI-MS untargeted metabolomics approach was applied and, by extracting the raw LC-MS data, a final dataset of 1414 *m/z* features was obtained. The resulting PCA score plot (Fig. 5A) showed a clear distinction between the biofouling samples according to the hydrodynamic conditions. Specifically, BA and BB samples were discriminated from BC samples along the first component (PC1, 69.1% of total variance), while BA samples were separated from BB samples along the second component (PC2, 10.4% of total variance).

A two-class PLS-DA model (high flow regime: BA/BB vs. low flow regime: BC) was then built to find differentially expressed chemomarkers depending on the hydrodynamic conditions. This PLS-DA model was used to determine the most discriminating m/z features. Metabolites with the highest VIP scores corresponded to those most differentially expressed between the two hydrodynamic conditions. Fig. 5B shows the expression of the 15 most discriminating chemomarkers (VIP score >2) in each sample. The putative annotation of these chemomarkers was carried out thanks to their MS/MS fragmentation pattern (interpretation and comparison with literature and specialized databases) and the use of the MN approach. All elements related to their annotation (database, molecular formula, observed ion, *m/z*, MS/MS fragmentation, MN cluster) were presented in Table S2.

3.5. Molecular networking and chemomarkers annotation

The MN consisted of 323 nodes (i.e., *m/z* features), most of which were clustered into 16 clusters of at least 3 nodes (labeled from A to P; Fig. 6). The combination between the MN and the analysis of the MS/MS spectra led to the putative annotation of 65 metabolites of the present dataset, including 12 of the 15 first VIPs (see Table S2). More precisely, the metabolites clustered in cluster A were hydrophobic compounds,

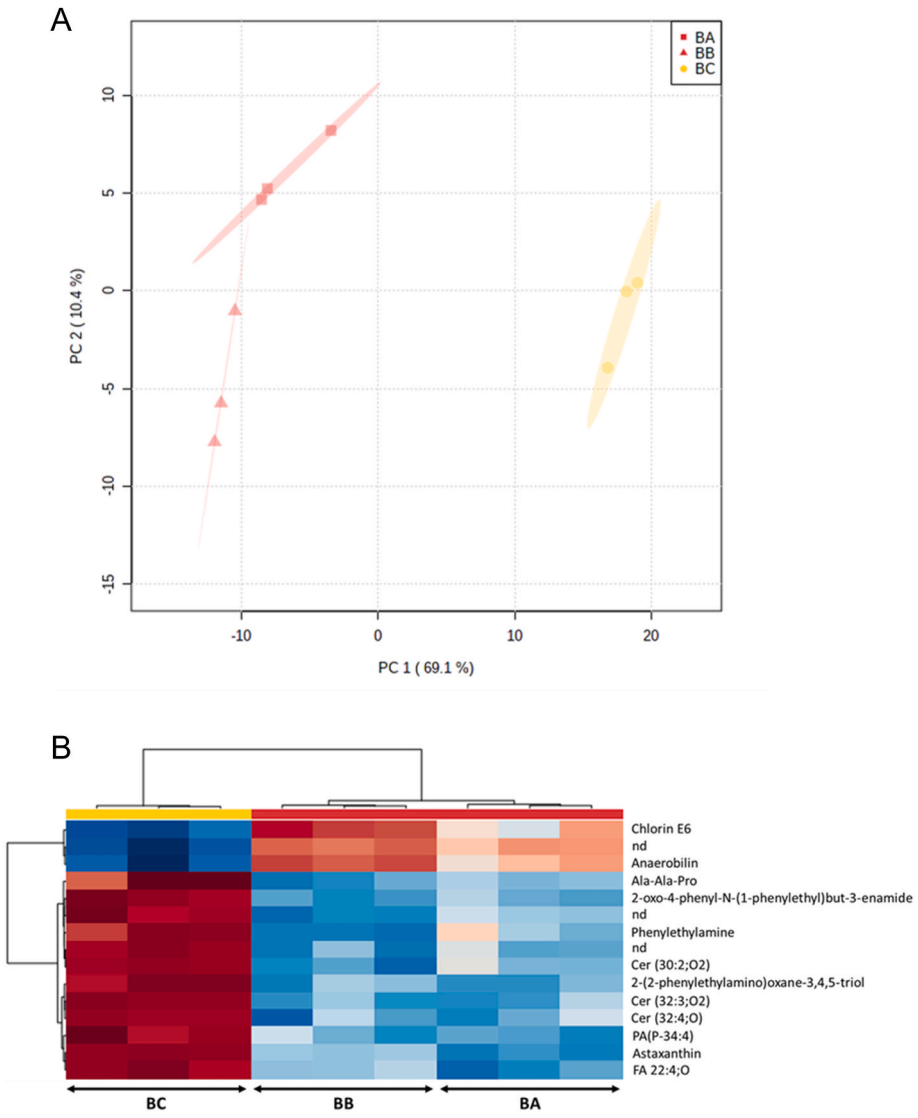

Fig. 5. Untargeted LC-MS-based metabolomics discrimination of biofouling samples formed in high and low flow regimes. (A) Principal component analysis (PCA) score plots of marine biofouling extracts obtained from LC-MS data grouped with the three conditions: high (red squares: BA and red triangles: BB) and low flow regimes (yellow circle BC). **(B)** Hierarchical Clustering Heatmaps using the top 15 PLS-DA VIPs ("nd": not defined). FA: Fatty acid; PA: Phosphatidic acid; Cer: Ceramide.

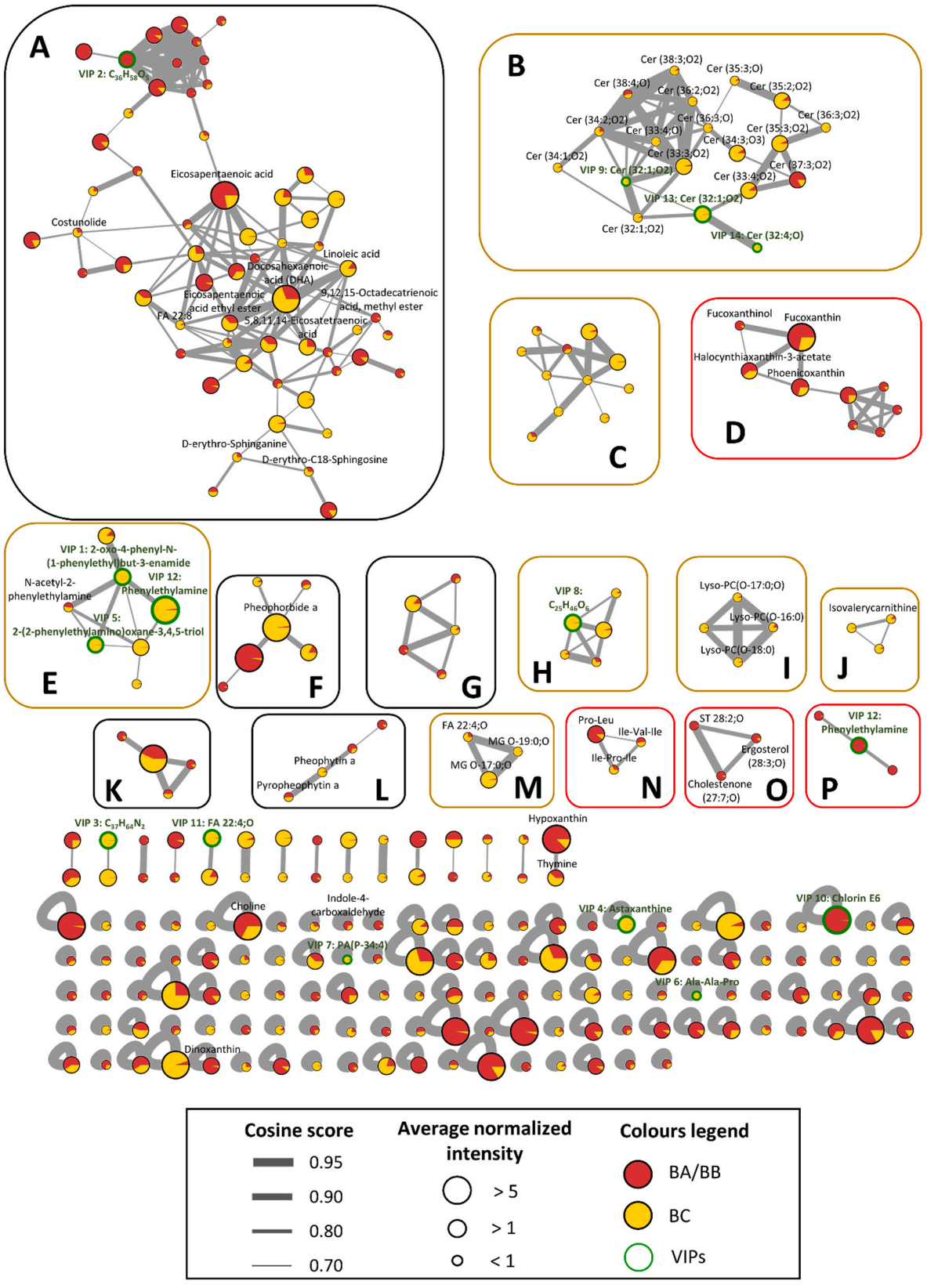

Fig. 6. Molecular network built with LC-MS/MS data of extracts of marine biofouling. Each node corresponds to a metabolite for which color ratios correspond to its relative abundances in the two hydrodynamic conditions (High: BA/BB samples in red; Low: BC samples in yellow) and the size corresponds to the normalized peak intensity. Some putatively annotations are given and discriminant compounds (VIPs) between the two hydrodynamic conditions are circled in green. FA: Fatty acid; PA: Phosphatidic acid; Cer: Ceramide; MG: Monoalkylglycerol; ST: Sterol; PC: Phosphatidylcholine.

such as fatty acids and derivatives, and most of them were specifically more expressed under one type of hydrodynamic conditions rather than another but without a general trend at the cluster level towards one of these two conditions. The unknown VIP n°2 ($C_{36}H_{58}O_5$) belonged to this cluster. Cluster B consisted of ceramides which were over-expressed under low hydrodynamic conditions (BC). In particular, 3 ceramides were included among the first 15 VIPs (VIPs n°9, 13 and 14; see Table S2). Unknown metabolites, more expressed in low hydrodynamic conditions (BC), were the main components of cluster C while several carotenoids, more expressed in high hydrodynamic conditions (BA/BB), were part of cluster D. Several phenylethylamine derivatives, including VIPs n°1, 6 and 12, formed cluster E and were characteristic of BC samples. Within clusters G, K and L, no clear differences between the two hydrodynamic conditions were observed, but within these clusters two chlorophyll *a* derivatives, pheophorbide a (cluster F) and pheophytin a (cluster L), were mainly expressed in BC samples. Clusters H, I, J and M were composed of metabolites also overexpressed in BC samples, including: (i) the unidentified VIP n°8 in cluster H, (ii) 3 *lyso*-phosphatidylcholines in cluster I, (iii) a carnitine derivative in cluster J and (iv) 2 monoacylglycerols and a fatty acid in cluster M. Clusters N, O and P collected metabolites mainly observed in BA/BB samples. More specifically, cluster N was composed of 3 peptides, while 3 steroids were found in cluster O and the heme degradation product, anaerobilin (VIP n°15), was putatively annotated in cluster P. Finally, 6 of the major VIPs were detected in clusters composed of two nodes or as self-loops (single nodes). Among them, chlorin E6 (VIP n°10) was mainly expressed in BA/BB samples while the others (VIPs n°3, 4, 6, 7, and 11) were mainly found in BC samples.

3.6. Biofilm quantity and chemical characterization of the EPS matrix

As expected from observation of the submerged panels (Fig. 1B), the amount of biofilm harvested increased under low hydrodynamic conditions, with a significant difference between BA or BB and BC ($p < 0.0001$) (Fig. S7). Conversely, the amount of colloidal EPS was significantly higher in BA than in BB and BC (Fig. 7). Variations in the total amounts of carbohydrates, uronic acids and proteins were determined for the two EPS fractions, namely colloidal and bound, and for the residual biofilm fraction. Irrespective of the site, the total carbohydrate content of the biofilms (all fractions taken together) was higher than the protein content (Fig. S8). Looking at the composition of biofilm matrix (EPS extracted in colloidal and bound fractions), the same trend was observed with a significant decrease ($p < 0.006$) in the carbohydrate/protein (C/P) ratio when panels were exposed to low hydrodynamic conditions (BC) compared to high hydrodynamic conditions (BA) (C/P ratios of 6.3 and 0.8 for BA and BC, respectively) (Fig. 7). For BC, the C/P ratio was even less than 1, indicating a predominant protein content of the matrix. Specifically, BC differed from the other two sites by higher proportions of protein ($p < 0.01$) in all fractions (colloidal, bound, and residual) (Fig. S8). Regarding the carbohydrate content, no significant difference was found between the sites ($p > 0.05$) regardless of the fraction. The same observation was made for uronic acid (UA) content in the colloidal and residual fractions, while in the bound fraction, BC samples had a higher proportion of UA than BA ($p = 0.03$) (Fig. S8).

Furthermore, a PCA of the different biofilm fractions at the three sites was performed based on the composition in proteins, carbohydrates, and UA (Fig. S9). Three clusters corresponding to the three sites were observed on the resulting score plot. BA and BC samples were discriminated along the first component, which accounted for 48.6% of the total variance. BC samples showed a more pronounced difference from the other two samples along the first component. Total protein content and, to a lesser extent, UA content in EPS were the most discriminative parameters for BC samples.

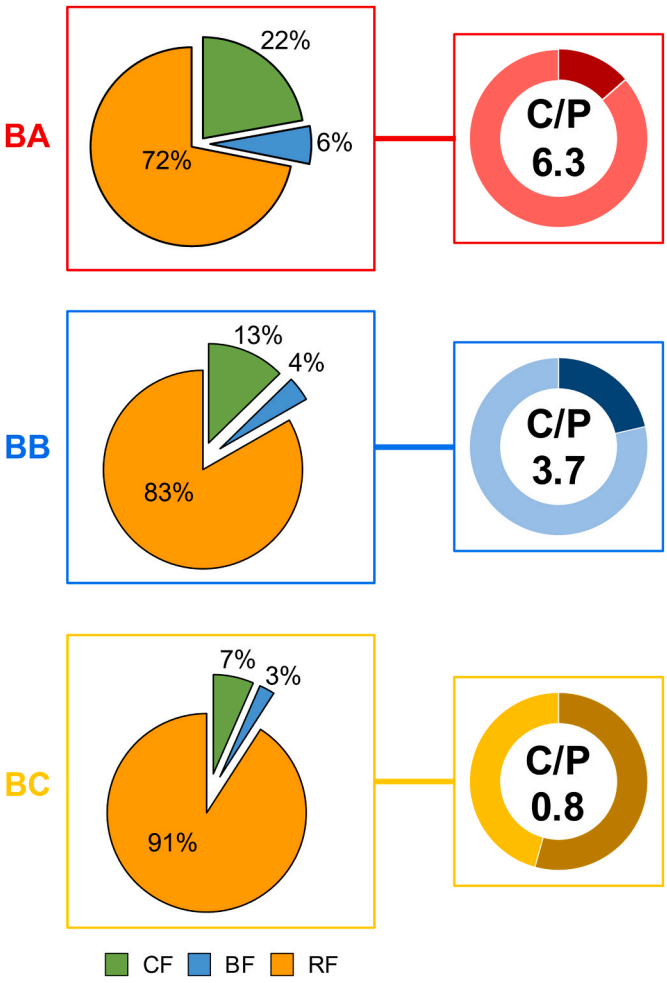

Fig. 7. Distribution (proportions in mass percent) of the different fractions (Colloidal and Bound Fractions as EPS fractions, and Residual Fraction) and Carbohydrate/Protein ratios in the biofouling samples collected at the 3 Etel sites (BA, BB, and BC). The left pie chart shows the mean percentage of each fraction, colloidal (green), bound (blue) and residual (yellow), across the three buoys. The doughnut chart on the right shows the average proportion of proteins (P) in dark color, and total carbohydrate amounts (C), in light color into each site. Carbohydrate/protein (C/P) ratios are shown within the doughnut chart. For more details see Table S4.

4. Discussion

In this study, we intend to understand how flow dynamics and turbulence affect the biofouling process in the Etel estuary in autumn. Hydrodynamics have rarely been studied in relation to biofouling. The use of an original approach using ADCP for flow characterization and a multi-omics approach (metabarcoding and metabolomics) coupled with biochemical analysis, allowed us to unravel links between taxonomic and metabolic biofouling adaptations and specificities of the Etel estuary.

4.1. Hydrodynamic behavior of the Etel estuary

The Etel site is primarily influenced by tidal patterns. Consequently, in cases where data cannot be collected simultaneously, the recommended approach is to perform a comparative analysis over the entire tidal cycle, encompassing the primary spring tide (full moon), neap tide, and secondary spring tide (new moon). This method has allowed us to maintain relevance when comparing hydrodynamics between different sites. However, local wind conditions may introduce slight tide

variations by influencing tides, especially through low tide exposure amplification. Conversely, low-pressure systems, which often associated with cloudy and rainy weather, can result in higher tides than predicted. These effects are mainly observed offshore, and the onshore location of the Etel test site makes their impact negligible. Additionally, river runoff resulting from heavy rainfall is another factor that can influence tidal patterns. We have not observed such events during our deployments.

The turbulence measured at BA, BB and BC was consistent with previous estimates derived from ADCP measurements collected in the center of the Sea Scheldt estuary, Belgium (Sentchev et al., 2020). The main difference in the hydrodynamic profile of BA, BB and BC was the flow velocity. In the center of the river (BA and BB), the mean and maximum flow velocities were 0.7–0.8 m/s and 2.4 m/s, respectively, similar to that evaluated in the center of the Sea Scheldt estuary, whereas the maximum velocity at Etel estuary is 70% higher (Fig. S10). The maximum velocities at the Etel estuary were observed during the ebb tide. During this phase of the tide, the flow converged due to the shape of the estuary, which resulted in flow acceleration and high velocities. During the flood stage of the tide, the flow crossed several bathymetric features, including a prominent ridge, before reaching BA and BB. The complex bathymetry generated friction and macro-turbulence near the bed, which then propagated upwards in the water column, causing flow deceleration and lower velocities. In BC, the low water depth and the proximity to the shore significantly limited the flow velocity during both ebb and flood, justifying a flow velocity about 3 times lower than that observed in BA and BB. The conditions at the Etel site allowed to conclude on the influence of mean velocity in providing different levels in the same global environment. However, the turbulence was globally homogeneous at the three points BA, BB and BC and consequently it was not possible to assess globally its specific influence on biofouling. The control of turbulence (velocity fluctuations) is complex, especially in natural environments, and dedicated experiments should be developed to study its influence separately for identical mean velocities. Therefore, the physical constraints applied to biofouling at our studied sites were mostly shear stress. However, these tidal conditions differ considerably from those of the riverine system and are characterized more by shear stresses varying between high and low values. Consequently, biofouling formation can also differ from the one established under steady currents (Chen et al., 2022).

4.2. Shear stress does not influence the composition of the core bacterial community but affects community structure

Our results showed that richness and diversity tended to be higher under high flow conditions, with a different community structure compared to that observed under low flow conditions. Previous studies have described similar trends in biofilm diversity but have not reliably linked the observed changes in bacterial communities to hydrodynamics (Chun et al., 2022; Simões et al., 2022; Tsagkari et al., 2022). Indeed, by modeling the effects of hydrodynamics on bacterial communities in river biofilms, Li et al. (2015) only concluded that diversity was higher in flowing water than in calm water. Conversely, Rickard et al. (2004) showed that a loss of diversity in a multi-species drinking water biofilm was associated with increasing shear stress from 0.12 to 0.26 m/s. The main reasons for the different diversity and structure of biofilms may be the different transport rates of nutrients, dissolved oxygen variations and cell adhesion, which influence biofilm formation and growth. Higher fluid velocity could promote nutrient and bacterial cell transport, which a positive effect on biofilm formation (Moreira et al., 2015; Thames et al., 2023), while stagnant or low flow conditions are a barrier to nutrient delivery and removal of waste components from the colony (Stewart, 2012), and also do not allow a good water oxygenation. However, very high shear stress conditions may prevent cell attachment or be responsible for cell detachment, making the biofilm thinner, as observed in this and other studies (Catão et al., 2019; Gomes and Mergulhão, 2021; Krsmanovic et al., 2021). A more integrated view of the effect of hydrodynamics on biofilms was given by Van Loosdrecht et al. (1995), who suggested that biofilm structure is determined by a balance between detachment and growth of biofilm communities. In other words, biofilm diversity could be promoted up to a certain flow rate, which was the case in the Etel estuary during our experiments but may be limited beyond that. This may in some way relate to the intermediate disturbance's hypothesis (Connell, 1978), which suggests that, in the context of patch dynamics (Wilson, 1994) relevant to surface colonization (Hutchinson et al., 2006; Molino et al., 2009), especially here when biofilms are exposed to fluids (Durham et al., 2012), the highest diversity will be reached with intermediate perturbation.

Thereafter, the main differences between the site communities were clearly related to the high abundance of an unknown genus among the *Pseudomonadales* in BC samples, which was the dominant group. *Pseudomonadales* have been reported as an extremely diverse and flexible group, including the genus *Endozoicomonas*. They have been reported to contain numerous symbionts of many marine sessile marine invertebrates, including corals, sponges, and cnidarians (Neave et al., 2017). The co-occurrence network analysis highlighted the close relationship between *Ectopleura* and *Oithona*, which could indicate symbiotic interactions with these two invertebrate genera. However, except for these taxa, the bacterial communities showed a very similar core composition across the three sites, with 237 genera in common accounting for over 98 % of the total number of reads. The taxonomic composition, dominated by the phyla *Bacteroidetes*, *Planctomycetes*, *Desulfobacterota*, *Verrucomicrobia,* has been previously reported to dominate biofilm assemblages (Djaoudi et al., 2022; Oberbeckmann et al., 2021). Nevertheless, this contrast with recent results by Catão et al. (2019) who observed changes in the taxonomic composition of marine prokaryotic biofilm communities when PVC panels were exposed to static versus highly dynamic conditions (15 knots, i.e., three times the velocities at BA and BB). One hypothesis could be that the flow velocities encountered at the three sites in the Etel estuary were already high enough to select for adapted bacterial taxa. Indeed, our datasets showed an enrichment of genera among *Flavobacteriaceae* (e.g., *Aquibacter*, *Lutimonas* and *Maribacter*) and *Rhodobacteriaceae* (e.g., *Boseongicola Sulfitobacter* and *Yoonia-Loktanella*) in samples exposed to high current, which may be better adapted to high hydrodynamic environments. Thus, our observations suggest that there is a stable and resilient core community under variations in the intensity of hydrodynamic conditions (*in-situ*). These observations are consistent with earlier study by Besemer et al. (2007), who showed that bacterial communities at different river velocities (from 0.065 m/s to 0.390 m/s) diverged from the initial community and converged to the same composition as the biofilm matured. One hypothesis would be that, as the Etel site is a highly dynamic environment subject to strong tidal currents (Thiébaut et al., 2022) biofilm communities may adapt to their environment through physiological or genomic adaptation mechanisms.

4.3. Eukaryote selection under hydrodynamic conditions

Our results showed that hydrodynamic conditions influence the structure and distribution of eukaryotes in marine biofouling. We found a higher number of metazoans in BC samples, 91% in total, compared to 46% and 5% in BA and BB samples, respectively. A high proportion of Cnidaria was observed in the BC samples, especially the genera *Ectopleura*. One species of this genera was affiliated: *Ectopleura larynx*. This colonial hydroid has generally been found in the Atlantic Ocean, particularly in sheltered areas with low tidal flow (Want et al., 2021), which is consistent with our observations. Also, *Ectopleura larynx* is known to dominate benthic assemblages in late autumn (October–November), which is again in line with our observations (Blöcher, 2013). Furthermore, we identified a lower number of ciliates in our samples. This contrasts with the study by Briand et al. (2018) in which investigated biofouling communities on artificial surfaces in Lorient (Atlantic). This difference could be explained by the hydrodynamics, which are

higher at Etel than in a harbor area (Lorient), and currents are known to prevent the installation of ciliates on surfaces (Risse-Buhl et al., 2009). Furthermore, given that we do not use the same primers, problems related to the choice of genetic markers could explain the underrepresentation of taxa, as recently suggested for eukaryotic biofouling communities (Portas et al., 2022).

As reported in the literature, hydrodynamics play a key role in larval dispersal and initial recruitment in the marine environments (Abelson and Denny, 1997; Koehl, 2007; Wheeler et al., 2019). Larval and spore dispersal is primarily dependent on local hydrodynamic characteristics, which, depending on their intensity, can export larvae far from the original population. However, water movement also affects the encounter of the propagule with the substrate and the attachment processes (Wheeler et al., 2019). Inevitably, unfavorable hydrodynamics can impede larval settlement, resulting in reduced settlement (Sahu et al., 2013), as observed in this study. However, hydrodynamics can also indirectly affect the larval settlement through its effect on microbial communities. For example, barnacle larvae show significantly greater attachment to a biofilm developed at high shear stress than to a biofilm grown at low shear stress (Neal et al., 1996). This is consistent with the presence of *Semibalanus* barnacles, which were found exclusively in BA samples in our study.

Furthermore, the results suggested that morphology is a determining factor for fouling colonization under hydrodynamic conditions. In particular, for sessile organisms which remain fixed, morphology has significant implications for their survival under strong hydrodynamic forces. This includes aspects such as shape, size, and texture of a biofouling organism, which can influence its resistance to shear stress (Gerard, 1987; Johnson and Koehl, 1994). This is particularly true for diatoms, whose abundance was higher in the high current samples, with the presence of the genera *Navicula* and *Nitzshia*. Moreover, the co-occurrence network highlighted the importance of diatoms in bacterial interactions in high currents. This highlights the significance of diatoms in shaping the microbial communities in these conditions. Remarkably, *Navicula* and *Nitzshia* genera have also been identified on ship coatings exposed to dynamic conditions at up to 10 knots (Hunsucker et al., 2014, 2016). This further highlighted their ability to survive and persist in high current environments. Additionally, these genera secrete large amounts of EPS as bacteria, and their two raphes enhance their adherence to surfaces (Christensen, 1991; Zargiel et al., 2011). Previous research has showed similar results, with biofouling communities exposed to dynamic conditions exhibiting higher adhesion and diatom abundance compared to those under static conditions (Zargiel and Swain, 2014). Furthermore, we observed that soft or mobile fouling organisms were more sensitive to high shear stress, namely *Ectopleura* (Cnidaria) and many copepods such as the genera *Oithona* and *Tachidius*. Indeed, the strong hydrodynamic forces exerted by Etel's tidal episodes constitute a powerful selective force on biofouling organisms, some of which do not have the adapted morphology to attach permanently to the substrate.

However, under high hydrodynamic conditions, mobile organisms are also found, including the planktonic copepod *Harpacticus* and the vagile ciliate *Heterohartmannula*. The same pattern was observed for the presence of some Endomyxa, including the genera *Vanella* and *Vampyrellida*. According to Antoniadou et al. (2011), species diversity and abundance of mobile fauna increased with increasing habitat complexity provided by the presence of sessile species. Although the proportion of these groups was low (<1,6% of reads), an associative relationship can be established between the abundance of these mobile groups and the presence of Ulvophyceae, among which the genus *Ulva* was the most abundant in samples exposed to strong hydrodynamics and which, according to the network analysis, presented a central role in interactions between bacteria. In this case, green algae may represent a temporary refuge for these species. These results are in agreement with those of Briand et al. (2018), who observed a positive correlation between the abundance of ciliates and the presence of Ulvophyceae in the harbour of Kernevel (26 km from Etel).

4.4. Hydrodynamic strengths influence biofilm quantity and EPS composition

Shear stress also had a significant effect on both biofilm abundance and EPS matrix composition, the latter being known to be produced by both bacteria and diatoms. The presence of hydrodynamic forces (BA/BB *vs*. BC) resulted in expected smoother biofilms, but also less abundant and less rich in proteins. In biofilms formed under hydrodynamic stress, we found that the proportion of matrix compounds (based on the amount of secreted EPS recovered in colloidal and bound fractions) was higher. Firstly, among these EPS, polysaccharides dominated, but without containing more UA for samples subjected to higher hydrodynamic stress. UA were quantified as their carboxyl groups known to provide binding sites for divalent cations, thus increasing the binding forces and structural stability of the biofilm matrix (Vu et al., 2009; Xu et al., 2018). Second, the proportion of EPS extracted in the colloidal fraction increased with increasing hydrodynamic forces. Since colloidal fractions contain the most soluble and loosely bound EPS of the matrix, high currents could eliminate them as more detachable EPS (Pierre et al., 2014). Here, under high shear stress, biofilm communities produced more colloidal EPS mainly under the nature of exopolysaccharides, which consequently establish sufficient interactions to form a mechanically stable and protective structure. High shear or turbulent flow conditions induce greater secretion of polysaccharides, which induce a better mechanical stability, and a more cohesive and resistant structure of biofilm, in addition to promoting initial cell adhesion to surfaces (Douterelo et al., 2013; Lemos et al., 2015; Wang et al., 2013). Chang et al. (2020) have related similar results under high shear stress with *Bacillius* spp. as an increasing EPS production was observed and was hypothesized to ensure robust cell adhesion. Thus, biofilms may be better able to resist higher shear forces, which tend to limit adhesion and increase breakout forces, by increasing the production of specific EPS, known to enhance cohesive forces within biofilms (Krsmanovic et al., 2021; Lemos et al., 2015; Paul et al., 2012). As the diatom composition seems to be more affected by shear stress than the bacterial one, it can be assumed that the same bacterial taxa change their EPS production and/or different diatom taxa express different EPS. A better characterization of EPS would be required to deepen the relative role of the different microbes of biofilms in the production of the EPS matrix.

4.5. Biofouling metabolome reflects the presence of specific eukaryote communities depending on the hydrodynamic conditions

Untargeted LC-MS-based metabolomics was used to assess whether contrasting hydrodynamics induced a metabolome shift at the community level. PLS-DA and molecular networking highlighted some putatively annotated metabolites which were specifically more detected in one of the two hydrodynamic conditions. Among the molecules predominantly found in BA/BB samples, three were steroids, including ergosterol. Ergosterol is the major fungal membrane sterol which regulates membrane fluidity (Yang et al., 2015). Several previous studies have used this compound to estimate fungal biomass in environmental samples. Furthermore, recent studies have reported the isolation of ergosterol from various marine fungi such as *Rhodotorula sphaerocarpa* (Salazar Alekseyeva et al., 2021), *Talaromyces* sp. (Lebeau et al., 2020) and *Phoma* sp. (Wu et al., 2018). The high expression of ergosterol in BA and BB samples was then consistent with the results obtained by metabarcoding, which showed a higher proportion of fungi in BA/BB samples compared to BC samples. In cluster D, 4 metabolites annotated as carotenoids were more highly expressed in BA/BB samples. The most abundant of them was annotated as fucoxanthin, a carotenoid mainly found in macroalgae, microalgae and diatoms (Peng et al., 2011; Xia et al., 2013). Fucoxanthin is the most important xanthophyll produced by Ochrophyta, and members of this division represented more than

34% of the sequences detected in BA samples and 59% in BB samples, whereas they represented only 3% in BC samples. More specifically, fucoxanthin has already been detected in most of the macroalgae of the genus *Ectocarpus*, which are mainly found in BA and BB samples, with an abundance of 20% and 14%, respectively (Lourenço-Lopes et al., 2021). Fucoxanthin is also abundant in unicellular microalgae (i.e., diatoms, class Bacillariophyta) (Brunet et al., 1996; Peng et al., 2011) and such taxa were predominantly found in BA/BB samples. Conversely, astaxanthin was specifically expressed in BC samples. Astaxanthin is a naturally occurring carotenoid pigment with strong antioxidant activity, commonly found in both crustaceans and macroalgae (Galasso et al., 2017; Weaver et al., 2018). The presence of this carotenoid could be correlated with the presence of *Ectopleura larynx*, which represents 70% in low hydrodynamic conditions compared to an average of 4% in high hydrodynamic conditions. This species has a bright red-orange coloration of its gonophores, which could be due to the accumulation of astaxanthin. Another hypothesis could come from the diet of hydroids, which consists mainly of crustaceans (containing astaxanthin), especially copepods and cladocerans (Blöcher, 2013). Nevertheless, astaxanthin accumulation could also reflect a seasonal variation related to the dominance of crustaceans and diatoms in summer and winter, respectively (Genzano, 2005). Lipids were also found to be more abundant in BC samples. Several lipid classes followed these findings, namely *lyso*-phosphatidylcholines (cluster I), monoacylglycerols (cluster M) and ceramides (cluster B). In this last cluster, 19 neutral glycosphingolipids have been annotated. Most of them have already been described in microalgae, including dinoflagellates, diatoms or haptophytes, invertebrates, cnidarians or some bacterial species (Li et al., 2017; Panevska et al., 2019). Lipids form the structural basis of cell membranes. They are also used as an energy reserve by all marine invertebrates, and they are among the most important organic compounds found in all marine invertebrates. Among them, fatty acids, monoalkyldiacylglycerols, triacylglycerols, glycerophospholipids and sphingolipids (Imbs et al., 2021) have already been described for their involvement in host-microbe interactions and for the role they play in mutualistic communication between cnidarians and *Symbiodinium* symbionts (Kitchen et al., 2017).

5. Conclusion

This multidisciplinary approach allowed a comprehensive characterization of biofouling by studying both the communities and their metabolic production through an untargeted metabolomics approach and the analysis of biochemical components of the biofilm matrix. Our findings revealed that hydrodynamic forces, particularly shear stress, shape the community structure, metabolite profiles, and the nature and quantity of biochemical components of the EPS matrix of biofilms that have been formed in the Etel estuary during autumn. The strong currents generated by the specific tidal regime of the Etel estuary were found to contribute to a higher overall diversity, with eukaryotic communities being particularly sensitive to hydrodynamic conditions. Symbionts of *Pseudomonadales* and their host *Ectopleura* were notably dominant under low shear stress conditions. Consequently, at high currents, the exopolymeric matrix which plays a crucial role in biofilm adhesion and cohesion consisted of six times more polysaccharides than proteins.

Funding

This work benefited from France Energies Marines and State financing managed by the National Research Agency under the Investments for the Future program bearing the reference ANR-10-IED-0006-32 and from the European Union's Horizon 2020 research and innovation program under the grant agreement 815180. This work was carried out in the frame of the ELEMENT and ABIOP + projects.

Data accessibility and benefit-sharing section

Raw data are also stored in the SRA (BioProject PRJNA883975) using the MIxS package.

Benefit-sharing statement

Benefits Generated: Benefits from this research accrue from the sharing of our data and results on public databases as described above.

CRediT authorship contribution statement

Aurélie Portas: Formal analysis, Writing - original draft. **Nathan Carriot:** Formal analysis, Writing - original draft. **Annick Ortalo-Magné:** Writing - revision and editing. **Guillaume Damblans:** Writing – review & editing. **Maxime Thiébaut:** Formal analysis, Writing - original draft. **Gérald Culioli:** Writing – review & editing. **Nolwenn Quillien:** Writing – review & editing. **Jean-François Briand:** Writing – review & editing.

Declaration of competing interest

The authors declare the following financial interests/personal relationships which may be considered as potential competing interests: Portas reports financial support was provided by French National Research Agency. Portas reports financial support was provided by Horizon Europe.

Data availability

Raw data are also stored in the SRA (BioProject PRJNA883975) using the MIxS package

Acknowledgments

The authors would like to than Chantier Bretagne Sud and Guinard Energies for their welcome and help in the field.

We are grateful to the Roscoff Bioinformatics platform ABiMS (http://abims.sb-roscoff.fr), part of the Institut Français de Bioinformatique (ANR-11-INBS-0013) and BioGenouest network, for providing help and/or computing and/or storage resources.

The authors thank Dr S. Greff (Aix-Marseille University, IMBE, France) for the LC-MS experiments which were conducted on the regional metabolomics platform MALLABAR [Funds: Institute of Ecology and Environment (INEE) of the French National Centre for Scientific Research (CNRS), Total Foundation and the French Sud-PACA regional council].

Appendix A. Supplementary data

Supplementary data to this article can be found online at https://doi.org/10.1016/j.marenvres.2023.106241.

References

Abelson, A., Denny, M., 1997. Settlement of marine organisms in flow. Annu. Rev. Ecol. Systemat. 28 (1), 317–339. https://doi.org/10.1146/annurev.ecolsys.28.1.317.

Antoniadou, C., Voultsiadou, E., Chintiroglou, C., 2011. Seasonal patterns of colonization and early succession on sublittoral rocky cliffs. J. Exp. Mar. Biol. Ecol. 403 (1), 21–30. https://doi.org/10.1016/j.jembe.2011.04.001.

Antunes, J., Leão, P., Vasconcelos, V., 2019. Marine biofilms: diversity of communities and of chemical cues. Environmental Microbiology Reports 11 (3), 287–305. https://doi.org/10.1111/1758-2229.12694.

Araújo, P.A., Malheiro, J., Machado, I., Mergulhão, F., Melo, L., Simões, M., 2016. Influence of flow velocity on the characteristics of *Pseudomonas fluorescens* biofilms. J. Environ. Eng. 142 (7), 04016031 https://doi.org/10.1061/(ASCE)EE.1943-7870.0001068.

Battin, T.J., Kaplan, L.A., Newbold, J.D., Cheng, X., Hansen, C., 2003. Effects of current velocity on the nascent architecture of stream microbial biofilms. Appl. Environ. Microbiol. https://doi.org/10.1128/AEM.69.9.5443-5452.2003.

Besemer, K., Singer, G., Limberger, R., Chlup, A.-K., Hochedlinger, G., Hödl, I., Baranyi, C., Battin, T.J., 2007. Biophysical controls on community succession in stream biofilms. Appl. Environ. Microbiol. 73 (15), 4966–4974. https://doi.org/10.1128/AEM.00588-07.

Blöcher, N.. *Biofouling in the Norwegian Salmon Farming Industry* [Doctoral thesis, Norges teknisk-naturvitenskapelige universitet, Fakultet for naturvitenskap og teknologi, Institutt for biologi]. https://ntnuopen.ntnu.no/ntnu-xmlui/handle/11250/245368.

Bokulich, N.A., Subramanian, S., Faith, J.J., Gevers, D., Gordon, J.I., Knight, R., Mills, D. A., Caporaso, J.G., 2013. Quality-filtering vastly improves diversity estimates from Illumina amplicon sequencing. Nat. Methods 10 (1), 57–59. https://doi.org/10.1038/nmeth.2276.

Briand, J.-F., Barani, A., Garnier, C., Réhel, K., Urvois, F., LePoupon, C., Bouchez, A., Debroas, D., Bressy, C., 2017. Spatio-temporal variations of marine biofilm communities colonizing artificial substrata including antifouling coatings in contrasted French coastal environments. Microb. Ecol. 74 (3), 585–598. https://doi.org/10.1007/s00248-017-0966-2.

Briand, J.-F., Pochon, X., Wood, S.A., Bressy, C., Garnier, C., Réhel, K., Urvois, F., Culioli, G., Zaiko, A., 2018. Metabarcoding and metabolomics offer complementarity in deciphering marine eukaryotic biofouling community shifts. Biofouling 34 (6), 657–672.

Brunet, C., Davoult, D., Casotti, R., 1996. Physiological reactions to a change in light regime in cultured *Skeletonema costatum* (Bacillariophyta): implications for estimation of phytoplankton biomass. Hydrobiologia 333 (2), 87–94. https://doi.org/10.1007/BF00017571.

Callahan, B.J., McMurdie, P.J., Rosen, M.J., Han, A.W., Johnson, A.J.A., Holmes, S.P., 2016. DADA2: high-resolution sample inference from Illumina amplicon data. Nat. Methods 13 (7). https://doi.org/10.1038/nmeth.3869. Article 7.

Carriot, N., Barry-Martinet, R., Briand, J.-F., Ortalo-Magné, A., Culioli, G., 2022. Impact of phosphate concentration on the metabolome of biofilms of the marine bacterium *Pseudoalteromonas lipolytica*. Metabolomics 18 (3), 18. https://doi.org/10.1007/s11306-022-01875-x.

Carriot, N., Paix, B., Greff, S., Viguier, B., Briand, J.-F., Culioli, G., 2021. Integration of LC/MS-based molecular networking and classical phytochemical approach allows in-depth annotation of the metabolome of non-model organisms—the case study of the brown seaweed *Taonia atomaria*. Talanta 225, 121925. https://doi.org/10.1016/j.talanta.2020.121925.

Catão, E.C.P., Pollet, T., Misson, B., Garnier, C., Ghiglione, J.-F., Barry-Martinet, R., Maintenay, M., Bressy, C., Briand, J.-F., 2019. Shear stress as a major driver of marine biofilm communities in the NW Mediterranean Sea. Front. Microbiol. https://doi.org/10.3389/fmicb.2019.01768, 0.

Chang, J., He, X., Bai, X., Yuan, C., 2020. The impact of hydrodynamic shear force on adhesion morphology and biofilm conformation of *Bacillus* sp. Ocean Eng. 197, 106860 https://doi.org/10.1016/j.oceaneng.2019.106860.

Chen, X., Zhang, C., Townend, I.H., Gong, Z., Feng, Q., Yu, X., 2022. The resilience of biofilm-bound sandy systems to cyclic changes in shear stress. Water Resour. Res. 58 (3) e2021WR031098. https://doi.org/10.1029/2021WR031098.

Chong, J., Soufan, O., Li, C., Caraus, I., Li, S., Bourque, G., Wishart, D.S., Xia, J., 2018. MetaboAnalyst 4.0: towards more transparent and integrative metabolomics analysis. Nucleic Acids Res. 46 (W1), W486-W494 https://doi.org/10.1093/nar/gky310.

Christensen, T., 1991. The diatoms. Biology and morphology of the genera. Phycologia 30 (2), 233–235. https://doi.org/10.2216/i0031-8884-30-2-233.1.

Chun, A.L.M., Mosayyebi, A., Butt, A., Carugo, D., Salta, M., 2022. Early biofilm and streamer formation is mediated by wall shear stress and surface wettability: a multifactorial microfluidic study. MicrobiologyOpen 11 (4), e1310. https://doi.org/10.1002/mbo3.1310.

Connell, J.H., 1978. Diversity in tropical rain forests and coral reefs. Science 199 (4335), 1302–1310. https://doi.org/10.1126/science.199.4335.1302.

D'Abzac, P., Bordas, F., Van Hullebusch, E., Lens, P.N.L., Guibaud, G., 2010. Extraction of extracellular polymeric substances (EPS) from anaerobic granular sludges: comparison of chemical and physical extraction protocols. Appl. Microbiol. Biotechnol. 85 (5), 1589–1599. https://doi.org/10.1007/s00253-009-2288-x.

Dang, H., Lovell, C.R., 2016. Microbial surface colonization and biofilm development in marine environments. Microbiol. Mol. Biol. Rev. 80 (1), 91–138. https://doi.org/10.1128/MMBR.00037-15.

Davidson, I., Cahill, P., Hinz, A., Major, R., Kluza, D., Scianni, C., Georgiades, E., 2023. Biofouling occlusion of ships' internal seawater systems: operational, economic, and biosecurity consequences. Biofouling 39 (4), 410–426. https://doi.org/10.1080/08927014.2023.2225411.

Djaoudi, K., Onrubia, J., Angel, T., Boukra, A., Guesnay, L., Portas, A., Barry-Martinet, R., Angeletti, B., Mounier, S., Lenoble, V., Briand, J.-F., 2022. Seawater copper content controls biofilm bioaccumulation and microbial community on microplastics. Sci. Total Environ. 814, 152278 https://doi.org/10.1016/j.scitotenv.2021.152278.

Dobretsov, S., Rittschof, D., 2020. Love at first taste : induction of larval settlement by marine microbes. Int. J. Mol. Sci. 21 (3), 731. https://doi.org/10.3390/ijms21030731.

Douterelo, I., Sharpe, R.L., Boxall, J.B., 2013. Influence of hydraulic regimes on bacterial community structure and composition in an experimental drinking water distribution system. Water Res. 47 (2), 503–516. https://doi.org/10.1016/j.watres.2012.09.053.

Durham, W.M., Tranzer, O., Leombruni, A., Stocker, R., 2012. Division by fluid incision: biofilm patch development in porous media. Phys. Fluids 24 (9), 091107. https://doi.org/10.1063/1.4747154.

Escudié, F., Auer, L., Bernard, M., Mariadassou, M., Cauquil, L., Vidal, K., Maman, S., Hernandez-Raquet, G., Combes, S., Pascal, G., 2018. Frogs : find, rapidly, OTUs with galaxy solution. Bioinformatics 34 (8), 1287–1294. https://doi.org/10.1093/bioinformatics/btx791.

Faust, K., Raes, J., 2016. CoNet app: inference of biological association networks using Cytoscape. F1000Research 5, 1519. https://doi.org/10.12688/f1000research.9050.2.

Flemming, Wingender, J., 2010. The biofilm matrix. Nat. Rev. Microbiol. 8 (9) https://doi.org/10.1038/nrmicro2415. Article 9.

Galasso, C., Corinaldesi, C., Sansone, C., 2017. Carotenoids from marine organisms: biological functions and industrial applications. Antioxidants 6 (4). https://doi.org/10.3390/antiox6040096. Article 4.

Gast, R.J., Dennett, M.R., Caron, D.A., 2004. Characterization of protistan assemblages in the Ross Sea, Antarctica, by denaturing gradient gel electrophoresis. Appl. Environ. Microbiol. 70 (4), 2028–2037. https://doi.org/10.1128/AEM.70.4.2028-2037.2004.

Genzano, G.N., 2005. Trophic ecology of a benthic intertidal hydroid, *Tubularia crocea*, at Mar del Plata, Argentina. J. Mar. Biol. Assoc. U. K. 85 (2), 307–312. https://doi.org/10.1017/S0025315405011197h.

Gerard, V.A., 1987. Hydrodynamic streamlining of *Laminaria saccharina* Lamour. In response to mechanical stress. J. Exp. Mar. Biol. Ecol. 107 (3), 237–244. https://doi.org/10.1016/0022-0981(87)90040-2.

Gomes, L.C., Mergulhão, F.J.M., 2021. A Selection of platforms to evaluate surface adhesion and biofilm formation in controlled hydrodynamic conditions. Microorganisms 9 (9). https://doi.org/10.3390/microorganisms9091993. Article 9.

Hunsucker, J.T., Hunsucker, K.Z., Gardner, H., Swain, G., 2016. Influence of hydrodynamic stress on the frictional drag of biofouling communities. Biofouling 32 (10), 1209–1221. https://doi.org/10.1080/08927014.2016.1242724.

Hunsucker, K.Z., Koka, A., Lund, G., Swain, G., 2014. Diatom community structure on in-service cruise ship hulls. Biofouling 30 (9), 1133–1140. https://doi.org/10.1080/08927014.2014.974576.

Hutchinson, N., Nagarkar, S., Aitchison, J.C., Williams, G.A., 2006. Microspatial variation in marine biofilm abundance on intertidal rock surfaces. Aquat. Microb. Ecol. 42 (2), 187–197. https://doi.org/10.3354/ame042187.

Johnson, A., Koehl, M., 1994. Maintenance of dynamic strain similarity and environmental stress factor in different flow habitats: thallus allometry and material properties of a giant kelp. J. Exp. Biol. 195 (1), 381–410. https://doi.org/10.1242/jeb.195.1.381.

Jones, A.-A.D., Buie, C.R., 2019. Continuous shear stress alters metabolism, mass-transport, and growth in electroactive biofilms independent of surface substrate transport. Sci. Rep. 9 (1) https://doi.org/10.1038/s41598-019-39267-2. Article 1.

Kastl, A., Bogler, A., Spinnler, M., Sattelmayer, T., Be'er, A., Bar-Zeev, E., 2020. Impact of hydrodynamics on the first stages of biofilm formation in forward osmosis with spacers. Environ. Sci. Technol. 54 (8), 5279–5287. https://doi.org/10.1021/acs.est.0c00380.

Kitchen, S.A., Poole, A.Z., Weis, V.M., 2017. Sphingolipid metabolism of a sea anemone is altered by the presence of dinoflagellate symbionts. Biol. Bull. 233 (3), 242–254. https://doi.org/10.1086/695846.

Koehl, M.R.A., 2007. Mini review: hydrodynamics of larval settlement into fouling communities. Biofouling 23 (5), 357–368. https://doi.org/10.1080/08927010701492250.

Krsmanovic, M., Biswas, D., Ali, H., Kumar, A., Ghosh, R., Dickerson, A.K., 2021. Hydrodynamics and surface properties influence biofilm proliferation. Adv. Colloid Interface Sci. 288, 102336 https://doi.org/10.1016/j.cis.2020.102336.

Lawes, J.C., Neilan, B.A., Brown, M.V., Clark, G.F., Johnston, E.L., 2016. Elevated nutrients change bacterial community composition and connectivity: high throughput sequencing of young marine biofilms. Biofouling 32 (1), 57–69. https://doi.org/10.1080/08927014.2015.1126581.

Lebeau, J., Petit, T., Fouillaud, M., Dufossé, L., Caro, Y., 2020. Alternative extraction and characterization of nitrogen-containing azaphilone red pigments and ergosterol derivatives from the marine-derived fungal *Talaromyces* sp. 30570 strain with industrial relevance. Microorganisms 8 (12), E1920. https://doi.org/10.3390/microorganisms8121920.

Lemos, M., Mergulhão, F., Melo, L., Simões, M., 2015. The effect of shear stress on the formation and removal of *Bacillus cereus* biofilms. Food Bioprod. Process. 93, 242–248. https://doi.org/10.1016/j.fbp.2014.09.005.

Leray, M., Yang, J.Y., Meyer, C.P., Mills, S.C., Agudelo, N., Ranwez, V., Boehm, J.T., Machida, R.J., 2013. A new versatile primer set targeting a short fragment of the mitochondrial COI region for metabarcoding metazoan diversity: application for characterizing coral reef fish gut contents. Front. Zool. 10 (1), 34. https://doi.org/10.1186/1742-9994-10-34.

Li, Y., Lou, Y., Mu, T., Ke, A., Ran, Z., Xu, J., Chen, J., Zhou, C., Yan, X., Xu, Q., Tan, Y., 2017. Sphingolipids in marine microalgae: development and application of a mass spectrometric method for global structural characterization of ceramides and glycosphingolipids in three major phyla. Anal. Chim. Acta 986, 82–94. https://doi.org/10.1016/j.aca.2017.07.039.

Li, Y., Wang, C., Zhang, W., Wang, P., Niu, L., Hou, J., Wang, J., Wang, L., 2015. Modeling the effects of hydrodynamic regimes on microbial communities within fluvial biofilms: combining deterministic and stochastic processes (world). ACS Publications; American Chemical Society. https://doi.org/10.1021/acs.est.5b03277 [Research-article].

Liu, Y., Tay, J.-H., 2002. The essential role of hydrodynamic shear force in the formation of biofilm and granular sludge. Water Res. 36 (7), 1653–1665. https://doi.org/10.1016/S0043-1354(01)00379-7.

Lourenço-Lopes, C., Fraga-Corral, M., Jimenez-Lopez, C., Carpena, M., Pereira, A.G., Garcia-Oliveira, P., Prieto, M.A., Simal-Gandara, J., 2021. Biological action mechanisms of fucoxanthin extracted from algae for application in food and

cosmetic industries. Trends Food Sci. Technol. 117, 163–181. https://doi.org/10.1016/j.tifs.2021.03.012.
Love, M.I., Huber, W., Anders, S., 2014. Moderated estimation of fold change and dispersion for RNA-seq data with DESeq2. Genome Biol. 15 (12), 550. https://doi.org/10.1186/s13059-014-0550-8.
Martin, M., 2011. Cutadapt removes adapter sequences from high-throughput sequencing reads. EMBnet.Journal 17 (1). https://doi.org/10.14806/ej.17.1.200. Article 1.
Marty, A., Schoefs, F., Damblans, G., Facq, J.-V., Gaurier, B., Germain, G., 2022. Experimental study of two kinds of hard marine growth effects on the hydrodynamic behavior of a cylinder submitted to wave and current loading. Ocean Eng. 263, 112194 https://doi.org/10.1016/j.oceaneng.2022.112194.
McMurdie, P.J., Holmes, S., 2013. phyloseq: an R Package for reproducible interactive analysis and graphics of microbiome census Data. PLoS One 8 (4), e61217. https://doi.org/10.1371/journal.pone.0061217.
Molino, P.J., Campbell, E., Wetherbee, R., 2009. Development of the initial diatom microfouling layer on antifouling and fouling-release surfaces in temperate and tropical Australia. Biofouling 25 (8), 685–694. https://doi.org/10.1080/08927010903089912.
More, T.T., Yadav, J.S.S., Yan, S., Tyagi, R.D., Surampalli, R.Y., 2014. Extracellular polymeric substances of bacteria and their potential environmental applications. J. Environ. Manag. 144, 1–25. https://doi.org/10.1016/j.jenvman.2014.05.010.
Moreira, J.M.R., Simões, M., Melo, L.F., Mergulhão, F.J., 2015. The combined effects of shear stress and mass transfer on the balance between biofilm and suspended cell dynamics. Desalination Water Treat. 53 (12), 3348–3354. https://doi.org/10.1080/19443994.2014.933625.
Nadell, C.D., Ricaurte, D., Yan, J., Drescher, K., Bassler, B.L., 2017. Flow environment and matrix structure interact to determine spatial competition in Pseudomonas aeruginosa biofilms. Elife 6, e21855. https://doi.org/10.7554/eLife.21855.
Neal, A.L., Simões, F.N., Yule, A.B., 1996. Interactions between shear rates and biofilms affecting exploratory behaviour by cyprids of *Elminius modestus* (Cirripedia). Mar. Biol. 127 (2), 241–246. https://doi.org/10.1007/BF00942109.
Neave, M.J., Michell, C.T., Apprill, A., Voolstra, C.R., 2017. *Endozoicomonas* genomes reveal functional adaptation and plasticity in bacterial strains symbiotically associated with diverse marine hosts. Sci. Rep. 7 (1) https://doi.org/10.1038/srep40579. Article 1.
Oberbeckmann, S., Bartosik, D., Huang, S., Werner, J., Hirschfeld, C., Wibberg, D., Heiden, S.E., Bunk, B., Overmann, J., Becher, D., Kalinowski, J., Schweder, T., Labrenz, M., Markert, S., 2021. Genomic and proteomic profiles of biofilms on microplastics are decoupled from artificial surface properties. Environ. Microbiol. 23 (6), 3099–3115. https://doi.org/10.1111/1462-2920.15531.
Oksanen, J., Kindt, R., Legendre, P., Hara, B., Simpson, G., Solymos, P., Henry, M., Stevens, H., Maintainer, H., Oksanen@oulu, jari, 2009. The Vegan Package.
Oursel, B., Garnier, C., Durrieu, G., Mounier, S., Omanović, D., Lucas, Y., 2013. Dynamics and fates of trace metals chronically input in a Mediterranean coastal zone impacted by a large urban area. Mar. Pollut. Bull. 69 (1), 137–149. https://doi.org/10.1016/j.marpolbul.2013.01.023.
Panevska, A., Skočaj, M., Križaj, I., Maček, P., Sepčić, K., 2019. Ceramide phosphoethanolamine, an enigmatic cellular membrane sphingolipid. Biochim. Biophys. Acta Biomembr. 1861 (7), 1284–1292. https://doi.org/10.1016/j.bbamem.2019.05.001.
Parada, A.E., Needham, D.M., Fuhrman, J.A., 2016. Every base matters: assessing small subunit rRNA primers for marine microbiomes with mock communities, time series and global field samples. Environ. Microbiol. 18 (5), 1403–1414. https://doi.org/10.1111/1462-2920.13023.
Paul, E., Ochoa, J.C., Pechaud, Y., Liu, Y., Liné, A., 2012. Effect of shear stress and growth conditions on detachment and physical properties of biofilms. Water Res. 46 (17), 5499–5508. https://doi.org/10.1016/j.watres.2012.07.029.
Peng, J., Yuan, J.-P., Wu, C.-F., Wang, J.-H., 2011. Fucoxanthin, a marine carotenoid present in brown seaweeds and diatoms: metabolism and bioactivities relevant to human health. Mar. Drugs 9 (10). https://doi.org/10.3390/md9101806. Article 10.
Pierre, G., Zhao, J.-M., Orvain, F., Dupuy, C., Klein, G.L., Graber, M., Maugard, T., 2014. Seasonal dynamics of extracellular polymeric substances (EPS) in surface sediments of a diatom-dominated intertidal mudflat (Marennes–Oléron, France). J. Sea Res. 92, 26–35. https://doi.org/10.1016/j.seares.2013.07.018.
Pluskal, T., Castillo, S., Villar-Briones, A., Orešič, M., 2010. MZmine 2: modular framework for processing, visualizing, and analyzing mass spectrometry-based molecular profile data. BMC Bioinf. 11 (1), 395. https://doi.org/10.1186/1471-2105-11-395.
Portas, A., Quillien, N., Culioli, G., Briand, J.-F., 2022. Eukaryotic diversity of marine biofouling from coastal to offshore areas. Front. Mar. Sci. 9. https://www.frontiersin.org/articles/10.3389/fmars.2022.971939.
Railkin, A.I., 2003. Marine Biofouling: Colonization Processes and Defenses. CRC Press. https://doi.org/10.1201/9780203503232.
REPHY, 2021. French observation and monitoring program for phytoplankton and hydrology in coastal waters. In: REPHY Dataset—French Observation and Monitoring Program for Phytoplankton and Hydrology in Coastal Waters. SEANOE. https://doi.org/10.17882/47248. Metropolitan data [jeu de données].
Rickard, A.H., McBain, A.J., Stead, A.T., Gilbert, P., 2004. Shear rate moderates community diversity in freshwater biofilms. Appl. Environ. Microbiol. 70 (12), 7426–7435. https://doi.org/10.1128/AEM.70.12.7426-7435.2004.
Risse-Buhl, U., Scherwass, A., Schlüssel, A., Arndt, H., Kröwer, S., Küsel, K., 2009. Detachment and motility of surface-associated ciliates at increased flow velocities. Aquat. Microb. Ecol. 55, 209–218. https://doi.org/10.3354/ame01302.
Sahu, G., Satpathy, K.K., Mohanty, A.K., Biswas, S., Achary, M.S., Sarkar, S.K., 2013. Larval abundance and its relation to macrofouling settlement pattern in the coastal waters of Kalpakkam, southeastern part of India. Environ. Monit. Assess. 185 (2), 1951–1967. https://doi.org/10.1007/s10661-012-2679-9.
Salazar Alekseyeva, K., Mähnert, B., Berthiller, F., Breyer, E., Herndl, G.J., Baltar, F., 2021. Adapting an ergosterol extraction method with marine yeasts for the quantification of oceanic fungal biomass. Journal of Fungi 7 (9). https://doi.org/10.3390/jof7090690. Article 9.
Schmidt, H., Thom, M., Wieprecht, S., Manz, W., Gerbersdorf, S.U., 2018. The effect of light intensity and shear stress on microbial biostabilization and the community composition of natural biofilms. Res. Rep. Biol. 9 (2018), 1–16. https://doi.org/10.15488/4904, 9.
Schultz, M.P., Bendick, J.A., Holm, E.R., Hertel, W.M., 2011. Economic impact of biofouling on a naval surface ship. Biofouling 27 (1), 87–98. https://doi.org/10.1080/08927014.2010.542809.
Sentchev, A., Thiébaut, M., Schmitt, F.G., 2020. Impact of turbulence on power production by a free-stream tidal turbine in real sea conditions. Renew. Energy 147, 1932–1940. https://doi.org/10.1016/j.renene.2019.09.136.
Simões, L.C., Gomes, I.B., Sousa, H., Borges, A., Simões, M., 2022. Biofilm formation under high shear stress increases resilience to chemical and mechanical challenges. Biofouling 38 (1), 1–12. https://doi.org/10.1080/08927014.2021.2006189.
Song, J., Beule, L., Jongmans-Hochschulz, E., Wichels, A., Gerdts, G., 2022. The travelling particles : community dynamics of biofilms on microplastics transferred along a salinity gradient. ISME Communications 2 (1). https://doi.org/10.1038/s43705-022-00117-4. Article 1.
Stewart, P.S., 2012. Mini-review: convection around biofilms. Biofouling 28 (2), 187–198. https://doi.org/10.1080/08927014.2012.662641.
Thames, H.T., Pokhrel, D., Willis, E., Rivers, O., Dinh, T.T.N., Zhang, L., Schilling, M.W., Ramachandran, R., White, S., Sukumaran, A.T., 2023. *Salmonella* biofilm formation under fluidic shear stress on different surface materials. Foods 12 (9). https://doi.org/10.3390/foods12091918. Article 9.
Thiébaut, M., Quillien, N., Maison, A., Gaborieau, H., Ruiz, N., MacKenzie, S., Connor, G., Filipot, J.-F., 2022. Investigating the flow dynamics and turbulence at a tidal-stream energy site in a highly energetic estuary. Renew. Energy 195, 252–262. https://doi.org/10.1016/j.renene.2022.06.020.
Tsagkari, E., Connelly, S., Liu, Z., McBride, A., Sloan, W.T., 2022. The role of shear dynamics in biofilm formation. NPJ Biofilms and Microbiomes 8, 33. https://doi.org/10.1038/s41522-022-00300-4.
Van de Peer, Y., De Rijk, P., Wuyts, J., Winkelmans, T., De Wachter, R., 2000. The European small subunit ribosomal RNA database. Nucleic Acids Res. 28 (1), 175–176. https://doi.org/10.1093/nar/28.1.175.
Van Loosdrecht, M.C.M., Eikelboom, D., Gjaltema, A., Mulder, A., Tijhuis, L., Heijnen, J. J., 1995. Biofilm structures. Water Sci. Technol. 32 (8), 35–43. https://doi.org/10.1016/0273-1223(96)00005-4.
Vu, B., Chen, M., Crawford, R.J., Ivanova, E.P., 2009. Bacterial extracellular polysaccharides involved in biofilm formation. Molecules 14 (7), 2535–2554. https://doi.org/10.3390/molecules14072535.
Wang, C., Miao, L., Hou, J., Wang, P., Qian, J., Dai, S., 2013. The effect of flow velocity on the distribution and composition of extracellular polymeric substances in biofilms and the detachment mechanism of biofilms. Water Sci. Technol. 69 (4), 825–832. https://doi.org/10.2166/wst.2013.785.
Wang, M., Carver, J.J., Phelan, V.V., Sanchez, L.M., Garg, N., Peng, Y., Nguyen, D.D., Watrous, J., Kapono, C.A., Luzzatto-Knaan, T., Porto, C., Bouslimani, A., Melnik, A. V., Meehan, M.J., Liu, W.-T., Crüsemann, M., Boudreau, P.D., Esquenazi, E., Sandoval-Calderón, M., et al., 2016. Sharing and community curation of mass spectrometry data with global natural products social molecular networking. Nat. Biotechnol. 34 (8) https://doi.org/10.1038/nbt.3597. Article 8.
Wang, Q., Garrity, G.M., Tiedje, J.M., Cole, J.R., 2007. Naïve bayesian classifier for rapid assignment of rRNA sequences into the new bacterial taxonomy. Appl. Environ. Microbiol. 73 (16), 5261–5267. https://doi.org/10.1128/AEM.00062-07.
Want, A., Bell, M.C., Harris, R.E., Hull, M.Q., Long, C.R., Porter, J.S., 2021. Sea-trial verification of a novel system for monitoring biofouling and testing anti-fouling coatings in highly energetic environments targeted by the marine renewable energy industry. Biofouling 37 (4), 433–451. https://doi.org/10.1080/08927014.2021.1928091.
Weaver, R.J., Cobine, P.A., Hill, G.E., 2018. On the bioconversion of dietary carotenoids to astaxanthin in the marine copepod, *Tigriopus californicus*. J. Plankton Res. 40 (2), 142–150. https://doi.org/10.1093/plankt/fbx072.
Wheeler, J.D., Secchi, E., Rusconi, R., Stocker, R., 2019. Not just going with the flow: the effects of fluid flow on bacteria and plankton. Annu. Rev. Cell Dev. Biol. 35 (1), 213–237. https://doi.org/10.1146/annurev-cellbio-100818-125119.
Wilson, J.B., 1994. The « intermediate disturbance hypothesis » of species coexistence is based on patch dynamics. N. Z. J. Ecol. 18 (2), 176–181.
Wu, H.-Y., Yang, F.-L., Li, L.-H., Rao, Y.K., Ju, T.-C., Wong, W.-T., Hsieh, C.-Y., Pivkin, M. V., Hua, K.-F., Wu, S.-H., 2018. Ergosterol peroxide from marine fungus *Phoma* sp. Induces ROS-dependent apoptosis and autophagy in human lung adenocarcinoma cells. Sci. Rep. 8 (1) https://doi.org/10.1038/s41598-018-36411-2. Article 1.
Xia, S., Wang, K., Wan, L., Li, A., Hu, Q., Zhang, C., 2013. Production, characterization, and antioxidant activity of fucoxanthin from the marine diatom *Odontella aurita*. Mar. Drugs 11 (7). https://doi.org/10.3390/md11072667. Article 7.
Xu, C., Zhang, S., Beaver, M., Lin, P., Sun, L., Doyle, S.M., Sylvan, J.B., Wozniak, A., Hatcher, P.G., Kaiser, K., Yan, G., Schwehr, K.A., Lin, Y., Wade, T.L., Chin, W.-C., Chiu, M.-H., Quigg, A., Santschi, P.H., 2018. The role of microbially-mediated exopolymeric substances (EPS) in regulating Macondo oil transport in a mesocosm experiment. Mar. Chem. 206, 52–61. https://doi.org/10.1016/j.marchem.2018.09.005.

Yang, H., Tong, J., Lee, C.W., Ha, S., Eom, S.H., Im, Y.J., 2015. Structural mechanism of ergosterol regulation by fungal sterol transcription factor Upc2. Nat. Commun. 6 (1) https://doi.org/10.1038/ncomms7129. Article 1.

Zargiel, K.A., Coogan, J.S., Swain, G.W., 2011. Diatom community structure on commercially available ship hull coatings. Biofouling 27 (9), 955–965. https://doi.org/10.1080/08927014.2011.618268.

Zargiel, K.A., Swain, G.W., 2014. Static vs dynamic settlement and adhesion of diatoms to ship hull coatings. Biofouling 30 (1), 115–129. https://doi.org/10.1080/08927014.2013.847927.